J Stat Phys (2013) 150:807–850
DOI 10.1007/s10955-012-0664-x

Threshold Saturation in Spatially Coupled Constraint Satisfaction Problems

S. Hamed Hassani · Nicolas Macris · Ruediger Urbanke

Received: 23 May 2012 / Accepted: 29 November 2012 / Published online: 14 December 2012

Abstract We consider chains of random constraint satisfaction models that are spatially coupled across a finite window along the chain direction. We investigate their phase diagram at zero temperature using the survey propagation formalism and the interpolation method. We prove that the SAT-UNSAT phase transition threshold of an infinite chain is identical to the one of the individual standard model, and is therefore not affected by spatial coupling. We compute the survey propagation complexity using population dynamics as well as large degree approximations, and determine the survey propagation threshold. We find that a clustering phase survives coupling. However, as one increases the range of the coupling window, the survey propagation threshold increases and saturates towards the phase transition threshold. We also briefly discuss other aspects of the problem. Namely, the condensation threshold is not affected by coupling, but the dynamic threshold displays saturation towards the condensation one. All these features may provide a new avenue for obtaining better provable algorithmic lower bounds on phase transition thresholds of the individual standard model.

Keywords Random constraint satisfaction · Survey propagation · Spin glass · Spatial coupling · Interpolation method

1 Introduction

The field of modern error correcting codes used on noisy communication channels has witnessed an interesting recent development. Spatially coupled Low-Density Parity-Check (LDPC) codes, initially introduced[1] by Felstrom and Zigangirov [1], have been recognized to have excellent performance due to the *threshold saturation phenomenon* [2]. We refer

[1] In its original form the construction goes under the name Terminated Convolutional Low-Density Parity-Check codes.

S. Hamed Hassani · N. Macris (✉) · R. Urbanke
Laboratory for Communication Theory, School of Computer and Communication Science, Ecole Polytechnique Fédérale de Lausanne, EPFL, Station 14, 1015 Lausanne, Switzerland
e-mail: nicolas.macris@epfl.ch

to [3, 4] for the history and review of contributions in the field of communications, and a general analysis of the phenomenon.

Recently we introduced an elementary statistical mechanical model, namely a chain of coupled Curie-Weiss spin systems [5, 6], that already captures all the main features of this phenomenon, and shows that it is related to basic concepts of statistical mechanics. In a nutshell, this model is a one-dimensional chain of complete graph Ising models coupled in the longitudinal direction[2] by a Kac-like potential. When the range of the Kac potential goes to infinity (and its intensity to zero) the spinodal curve is pushed towards the coexistence one. The stable phase undergoes nucleation and grows, starting from the ends of the chain, and consequently (in the Kac limit) the metastability domain disappears from the phase diagram. This has important algorithmic consequences in the context of error correcting codes, for the recovery of an original message from the corrupted one.

We already argued in [5, 6] that threshold saturation occurs quite generally when mean field models are coupled together into a one-dimensional chain and the longitudinal range of the coupling increases to infinity. The individual mean field model may be some sort of spin glass system on a sparse Erdös-Rényi like random graph or on a complete graph (or on a hyper-graph). The sparse case is relevant to error correcting codes; see [3] and references therein. The case of complete graphs is relevant to compressive sensing, another topic to which these ideas have been successfully applied [9–11].

Among other models, defined on sparse random graphs, that are of great interest both in theoretical computer science and statistical mechanics, are random Constraint Satisfaction Problems (CSP). We refer the reader who is not familiar with such problems to the recent book [12]. In this paper we investigate *random spatially coupled-CSP*. We specifically concentrate on two main representatives: satisfiability (SAT) and coloring (COL). We also briefly discuss the XOR-SAT problem which is somewhat similar to the LDPC codes on the binary erasure channel, but has an interest of its own.

Here we focus on the *zero-energy* states of CSP. There are two ways to formulate the problem. One can directly minimize the Hamiltonian, or one can study the uniform measure over zero-energy states. We will focus essentially on the first aspect. The second one will only be briefly discussed. We say that a SAT (resp. UNSAT) phase corresponds to a vanishing (resp. finite) average ground state energy per variable, in the thermodynamic limit. Since the ground state energy per variable concentrates, this means that in a SAT (resp. UNSAT) phase there are, with high probability, at most a sub-linear (resp. at least a linear) number of unsatisfied constraints. In the language of computer science the problems that we are investigating are randomized versions of MAX-SAT and MAX-COL.

Coupled-CSP are based on chains of L *individual* random bipartite graphs with constant degree K for constraint nodes, and Poisson degree with mean αK for variable nodes. Each individual bipartite graph is appropriately *coupled* to its neighbors across a window of size w. The precise construction is explained in detail in Sect. 2. The number $\alpha > 0$ is a measure of the constraint density in the bulk of the chain, and plays the role of a control parameter. In the K-SAT problem each constraint corresponds to satisfying a disjunction of K literals. In Q-COL, constraint nodes have degree 2 and all variable nodes connected to the same constraint node must have different colors in a Q-ary alphabet. Despite the similarities in construction with the LDPC case, in general, CSP (and coupled-CSP) are considerably more difficult to analyze. To study the ground state problem we adopt the *Survey Propagation* (*SP*) *formalism*, which is derived from the zero-temperature (level-1) cavity method of

[2]Similar models have already been considered in other contexts [7, 8].

spin-glass theory [13]. We refer to [12] for a recent pedagogical account, but for the convenience of the reader we review and adapt the formalism to coupled CSP, in a streamlined form, in Appendix B.

Let us pause and explain the predictions of the SP formalism for individual graph ensembles [14, 15]. SP is a sophisticated mean field theory based on a set of fixed point equations. They predict the existence of a SAT-UNSAT phase transition when α crosses a critical threshold α_s. At a lower value $\alpha_{\rm SP}$ one finds a bifurcation from trivial to non-trivial solution of the fixed point equations. In the interval $[\alpha_{\rm SP}, \alpha_s]$ the solution space is fragmented in an exponentially large (in system size) number of well separated clusters of SAT ground states in Hamming space (binary or Q-ary). The rate of growth of the number of such clusters with system size, is called the *zero-energy complexity* and is positive in the interval $[\alpha_{\rm SP}, \alpha_s]$. The complexity goes to zero at α_s and becomes formally negative above α_s.

We consider the SP equations for coupled K-SAT and Q-coloring models and solve them by the method of population dynamics (Sects. 3 and 4). We find a positive complexity in an interval $[\alpha_{{\rm SP},L,w}, \alpha_{s,L,w}]$ which allows to determine the SAT-UNSAT phase transition point $\alpha_{s,L,w}$ (where the complexity becomes formally negative). We make the following observations for the interval where the complexity is positive. We have that $\alpha_{s,L,w} > \alpha_s$ and $\alpha_{s,L,w} \downarrow \alpha_s$ as L increases (and w fixed). Interestingly we find that *threshold saturation takes place*, namely $\alpha_{{\rm SP},L,w} \to \alpha_s$ as L and w both increase such that $1 \ll w \ll L$. These findings are supported by a large K and Q analysis of the SP fixed point equations of coupled CSP (Sects. 3 and 4). In this limit the fixed point equations reduce to one-dimensional difference equations, analogous to the ones found for the Curie-Weiss chain or coupled LDPC codes on the binary erasure channel. This allows to study an "average total warning probability" that characterizes the phase of the system. This quantity is somewhat analogous to the average magnetization in the CW chain, or the average erasure probability for LDPC codes. A corresponding "van der Waals curve" displays an oscillating structure around a "Maxwell plateau". Each oscillation corresponds to a state of the system characterized by a kink profile for a "local warning density" and a "local complexity density" along the chain.

Perfect threshold saturation $\alpha_{{\rm SP},L,w} \to \alpha_s$ only occurs in the regime $L, w \to +\infty$ with $1 \ll w \ll L$. We take $L \to +\infty$ in order that the bulk constraint density becomes insensitive to the boundary. It is perhaps less clear that one should also take $w \to +\infty$ (after $L \to +\infty$) so let us briefly comment on this aspect. The kinks alluded to in the previous paragraph are minimizers of a complexity functional. In the framework of the cavity method this functional is a thermodynamic potential, so when a kink is displaced from one equilibrium position to the neighboring one along the chain, this incurs a thermodynamic or complexity cost. Since the transition width of the kinks is of the order of w, this cost vanishes in the limit $w \to +\infty$ corresponding to a continuum limit. This explains why the total complexity remains positive in a small interval $[\alpha_{{\rm SP},w}, \alpha_s]$ which shrinks down to zero as $w \to +\infty$. The situation is analogous to the CW chain where it was calculated that the free energy cost for the kink displacement is a kind of Peierls-Nabarro barrier of height $O(e^{-cw})$ for the motion of solitons on lattices [6].

The thermodynamic limits of the average ground state energies per node, for the chain and the individual ensembles are proven to be equal (Sect. 5). The proof uses an interpolation method [16–18] in a convenient combinatorial form similar to [19]. This result is of some importance because it establishes that non-analytic (phase transition) points in the average ground state energy per node of the chain and individual ensembles, occur at the same constraint density. In other words one has $\lim_{L\to+\infty} \alpha_{s,L,w} = \alpha_s$.

In Sects. 6 and 7 we briefly discuss further important aspects that will be the object of more detailed future work.

The SP formalism says nothing about the relative sizes (internal entropy) of clusters of solutions and does not take into account which of them are "relevant" to the uniform measure over zero energy solutions. This issue is addressed by the entropic cavity method [20–23] which allows to compute the so-called dynamical and condensation thresholds α_d and α_c. We have computed the dynamical $\alpha_{d,L,w}$ and condensation $\alpha_{c,L,w}$ thresholds of coupled CSP, and observe that as L increases $\lim_{L\to+\infty}\alpha_{c,L,w}\to\alpha_c$ (w fixed) while $\alpha_{d,L,w}\to\alpha_c$ when both w and L increase in the regime $1\ll w\ll L$. The first observation is consistent with a rigorous result proved in Appendix A: the thermodynamic limit of the free energy (at finite temperature) of the chain is identical to that of the individual model. These issues are discussed in Sect. 6.

This work may have interesting algorithmic consequences. Any lower bound on $\alpha_{s,L,w}$ can be turned into a lower bound for α_s by taking $L\to+\infty$ (note this is also true for the condensation threshold). In particular, algorithmic lower bounds on $\alpha_{s,L,w}$ can be turned into lower bounds for α_s. Now, because of the saturation of the SP and dynamical thresholds of coupled CSP, the values of α for which the space of zero-energy solutions is fragmented into well separated clusters, are substantially larger, compared to values of individual ensembles. Therefore one may hope that a form of *algorithmic threshold saturation*, or at least *algorithmic threshold increase*, happens for some well chosen algorithms applied to coupled CSP. This may allow to *prove* better algorithmic lower bounds on $\alpha_{s,L,w}$ and thus α_s. The proposed methodology is briefly discussed and illustrated in Sect. 7 with simple peeling algorithms.

2 General Setting

We define a general class of CSP that form the *individual ensemble*. Then we couple these, to form one-dimensional chains called *spatially coupled-CSP ensembles*.

2.1 Individual CSP Ensemble $[N, K, \alpha]$

First, we specify an ensemble (N, K, α) of random bipartite graphs. Let $G = (V \cup C, E)$ with *variable* nodes $i \in V$, *constraint* nodes $c \in C$ and edges $\langle c, i\rangle$ connecting sets C and V. We have $|V| = N$, $|C| = M$, where $M = \lfloor \alpha N \rfloor$ (the integer part of αM) and α is a fixed number called the constraint density. We call N the size of the graph which is to be thought as large, $N\to+\infty$. All constraints c have degree K, and each edge $\langle c, i\rangle$ emanating from c is independently connected uniformly at random (u.a.r.) to a node in $i \in V$. As $N\to+\infty$, the degrees of the variable nodes tend to independent identically distributed (i.i.d.) with distribution Poisson(αK).

We denote by ∂i the set of constraints connected to variable node i and by ∂c the set of variable nodes connected to a constraint c.

For each graph G of the ensemble $[N, K, \alpha]$ we define a Hamiltonian (or cost function). To the variable nodes $i \in V$ we attach variables $x_i \in \mathcal{X}$ taking values in a discrete alphabet $\mathcal{X}$. To each constraint $c \in C$ we associate a function $\psi_c(x_{\partial c})$ which depends only on the variables $x_{\partial c} = (x_i)_{i\in\partial c}$ connected to c. For constraint satisfaction problems $\psi_c(x_{\partial c}) \in \{0, 1\}$; we say that the constraint is *satisfied* if $\psi_c(x_{\partial c}) = 1$ and *not satisfied* if $\psi_c(x_{\partial c}) = 0$. The total Hamiltonian is

$$\mathcal{H}(\underline{x}) = \sum_{c\in C}\big(1 - \psi_c(x_{\partial c})\big). \tag{1}$$

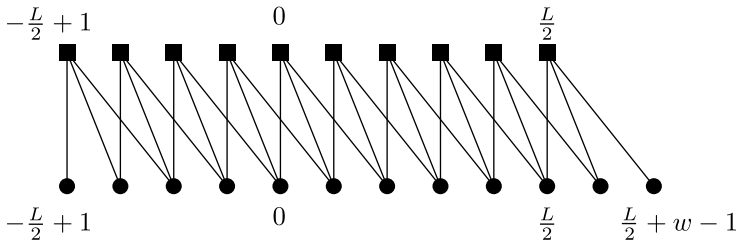

Fig. 1 A representation of the geometry of the graphs with window size $w = 3$ along the "longitudinal chain direction" z. The "transverse direction" is viewed from the *top*. At each position there is a stack of N variable nodes (*circles*) and a stack M constraint nodes (*squares*). The depicted links between constraint and variable nodes represent stacks of edges

For many problems of interest the functions ψ_c are themselves random. This will be made precise in each specific example; the only important condition is that the functions ψ_c are i.i.d. for all $c \in C$. The ground state energy is $\min_{\underline{x}} \mathcal{H}(\underline{x})$, the minimum possible number of unsatisfiable constraints. Our main interest is in the average ground state energy per node

$$e_N(\alpha) = \frac{1}{N}\mathbb{E}\Big[\min_{\underline{x}} \mathcal{H}(\underline{x})\Big] \tag{2}$$

where the expectation is taken over the $[N, K, \alpha]$ ensemble and possibly over the randomness of ψ_c.

2.2 Coupled-CSP Ensemble $[N, K, \alpha, w, L]$

This ensemble represents a chain of coupled underlying ensembles. Figure 1 is a visual aid but gives only a partial view. We align positions $z \in \mathbb{Z}$. On each position $z \in \mathbb{Z}$, we lay down N variable nodes labeled $(i, z) \in V_z$, $i = 1, \ldots, N$. We also lay down $M = \lfloor \alpha N \rfloor$ check nodes labeled $(c, z) \in C_z$, $c = 1, \ldots, M$. When the node labels are used as subscripts, say as in $a_{(i,z)}$ or $a_{(c,z)}$, we will simplify the notation to a_{iz} or a_{cz}. Let us now specify how the set of edges, E, is chosen. Each constraint (c, z) has degree K, in other words K edges emanate from it. Each of these K edges is connected to variable nodes as follows: we first pick a position $z + k$ with k uniformly random in the window $\{0, \ldots, w - 1\}$, then we pick a node $(i, z+k)$ u.a.r. in V_{z+k}, and finally we connect (c, z) to $(i, z+k)$. The set of edges emanating from (i, z) can be decomposed as a union $\bigcup_{k=0}^{w-1} \{\langle (c, z-k), (i, z)\rangle \mid c \in C_z\}$. Asymptotically as $N \to +\infty$, its cardinality is Poisson(αK); and the cardinalities of each set in the union are i.i.d. Poisson$(\frac{\alpha K}{w})$.

Finally, take L an even integer. Restrict the set of constraint nodes to $\bigcup_{z=-\frac{L}{2}+1,\ldots,+\frac{L}{2}} C_z$ and delete edges emanating from constraints that do not belong to this set. Restrict the set of variable nodes to $\bigcup_{z=-\frac{L}{2}+1,\ldots,\frac{L}{2}+w-1} V_z$.

As in Sect. 2.1, we have a set of variables $x_{iz} \in \mathcal{X}$ and constraint functions $\psi_{cz}(x_{\partial cz})$ taking values in $\{0, 1\}$. To each coupled graph in the ensemble we associate the Hamiltonian depending on $\underline{x} = (x_{iz})$, $(i, z) \in \bigcup_{z=-\frac{L}{2}+1,\ldots,\frac{L}{2}+w-1} V_z$,

$$\mathcal{H}_{\mathrm{cou}}(\underline{x}) = \sum_{z=-\frac{L}{2}+1}^{\frac{L}{2}} \sum_{c \in C_z} \big(1 - \psi_{cz}(x_{\partial(cz)})\big). \tag{3}$$

The minimum over $\underline{x}$ is the ground state energy and its ensemble average per node is

$$e_{N,L,w}(\alpha) = \frac{1}{NL}\mathbb{E}\Big[\min_{\underline{x}} \mathcal{H}_{\text{cou}}(\underline{x})\Big], \tag{4}$$

where $\mathbb{E}$ is over the $[N, K, \alpha, w, L]$ graph ensemble and on the randomness in ψ_{cz}.

Remark about the constraint density In this paper we have adopted the constraint density of the underlying ensemble α as our control parameter. *For a chain of coupled ensembles it represents the density of constraints in the bulk*. More precisely, for a chain of length L the ratio of the total number of constraints to the total number of nodes is $\frac{ML}{NL+N(w-1)}$ (see Fig. 1). This means that the average density of constraints is $\alpha_{\text{av}}(L, w) = \alpha\frac{L}{L+w-1} < \alpha$. This tends to α as $L \to +\infty$ so that in this limit the average density becomes insensitive to the boundary. In the present context, the spatial structure makes it more natural to take the bulk rather than the average density as a control parameter.

Remark about the boundary conditions In the formulation above we have free boundary conditions. However, the average degree of the variable nodes close to the boundaries is reduced so that the CSP is *easier to solve close to the boundaries*. Variable nodes close to the right boundary $z = \frac{L}{2}+1, \ldots, \frac{L}{2}+w-1$ have degrees Poisson$(\frac{\alpha K}{w}(\frac{L}{2}+w-z))$, and those close to the left boundary $z = -\frac{L}{2}+1, \ldots, -\frac{L}{2}+w-1$ have degrees Poisson$(\frac{\alpha K}{w}(z+\frac{L}{2}))$. It is sometimes convenient to imagine that the boundary nodes are connected to "satisfied extra constraint nodes", and all have Poisson(αK) degree.

2.3 K-Satisfiability and Q-Coloring

We define the main examples of constraint satisfaction problems that we analyze in this paper.

The K-SAT Problem The individual system is defined as follows. We take $x_i \in \{0, 1\}$ the Boolean alphabet. Set $n(x_i) \equiv \bar{x}_i$ for the negation operation, and define $n^d(x_i) \equiv x_i$ when $d = 0$ and $n^d(x_i) \equiv n(x_i) = \bar{x}_i$ when $d = 1$. Pick Bernoulli$(\frac{1}{2})$ i.i.d. numbers $d_{\langle c,i\rangle}$ for each edge $\langle c, i\rangle \in E$. We say that an edge is *dashed* when $d_{\langle c,i\rangle} = 1$ and *full* when $d_{\langle c,i\rangle} = 0$. With this convention, a variable in a constraint is negated when it is connected to a dashed edge, and is not negated when it is connected to a full edge. We set

$$\psi_c(x_{\partial c}) = \mathbb{1}\Big(\bigvee_{i\in\partial c}\big(n^{d_{\langle c,i\rangle}}(x_i)\big) = 1\Big). \tag{5}$$

These definitions are extended to the coupled system in an obvious way

$$\psi_{cz}(x_{\partial(cz)}) = \mathbb{1}\Big(\bigvee_{iu\in\partial(cz)}\big(n^{d_{\langle cz,iu\rangle}}(x_{iu})\big) = 1\Big), \tag{6}$$

where the important point is that $d_{\langle cz,iu\rangle}$ are i.i.d. Bernoulli$(\frac{1}{2})$ for all edges. The ground state energy counts the minimum possible number of unsatisfiable constraints. The instance is satisfiable iff the ground state energy is equal to zero.

The Q-COL Problem For the individual ensemble, we take $x_i \in \mathcal{X} = \{0, \ldots, Q-1\}$ the Q-ary color alphabet, $K = 2$ for the constraint node degrees, and

$$\psi_c(x_{\partial c}) = \mathbb{1}\big(x_i \neq x_j \text{ for } \{i, j\} = \partial c\big). \tag{7}$$

Since the constraints have degree 2 one can replace them by edges connecting directly i and j for $i, j \in \partial c$. The induced graph is, in the large size limit, equivalent to the Erdös-Rényi random graph $G(N, \frac{2\alpha}{N})$. The constraint (7) forbids two neighboring nodes to have the same color.

These definitions are easily extended to the coupled system. The induced graph (obtained by replacing constraints by edges) is now a coupled chain of Erdös-Rényi graphs. In place of (7) we take $x_{iz} \in \mathcal{X} = \{0, \dots, Q-1\}$ and

$$\psi_{cz}(x_{\partial(cz)}) = \mathbb{1}\big(x_{iu} \neq x_{jv} \text{ for } \big\{(i,u),(j,v)\big\} = \partial(c,z)\big). \tag{8}$$

Given an instance of the induced graph, the ground state energy counts the minimum possible number of edges with vertices of the same color. The graph is colorable iff this number is zero.

The K-XORSAT Problem We briefly give relevant definitions that will be used in Sect. 7 and Appendix A. For the individual system $x_i \in \{0,1\}$ and $\psi_c(x_{\partial c}) = \mathbb{1}(\bigoplus_{i\in\partial c} x_i = b_c)$ with b_c being i.i.d. Bernoulli($\frac{1}{2}$). Similarly for the coupled system $\psi_{cz}(x_{\partial(cz)}) = \mathbb{1}(\bigoplus_{iu\in\partial(cz)} x_{iu} = b_{cz})$ with b_{cz} being i.i.d. Bernoulli($\frac{1}{2}$).

2.4 Static Phase Transition Threshold

For the purpose of analysis, it is useful to also consider an ensemble of coupled graphs with *periodic* boundary conditions. This ensemble is simply obtained from the $[N, K, \alpha, w, L]$ ensemble by identifying the variable nodes (i, z) at positions $z = \frac{L}{2} + k$ with nodes (i, z) at positions $z = -\frac{L}{2} + k$ for each $k = 1, \dots, w-1$. The formal expression of the Hamiltonian $\mathcal{H}^{\text{per}}_{\text{cou}}(\underline{x})$ is the same as in (3) except that now $\underline{x} = (x_{iz})$ with $\bigcup_{z=-\frac{L}{2}+1,\dots,\frac{L}{2}} V_z$. Quantities pertaining to this ensemble will be denoted by a superscript "per".

Theorem 1 (Comparison of open and periodic chains) *For the general coupled-CSP* $[N, K, \alpha, w, L]$ *ensembles we have*

$$e^{\text{per}}_{N,L,w}(\alpha) - \frac{\alpha w}{L} \leq e_{N,L,w}(\alpha) \leq e^{\text{per}}_{N,L,w}(\alpha). \tag{9}$$

This theorem has an easy proof given in Sect. 5.

The next theorem does not have a trivial proof and is stated here for the special cases of K-SAT and Q-COL. While it is presumably valid for many other CSP's, we do not expect that it should hold in complete generality. For example it is well known from models in other areas of statistical and condensed matter physics that the ground states of a periodic chain can break translation invariance (e.g. crystals develop non-trivial periodic patterns) and then have lower energy than the homogeneous ground state. If this happens the statement of the theorem cannot possibly hold.

Theorem 2 (Thermodynamic limit) *For the* K*-SAT and* Q*-COL models the two limits* $\lim_{N\to+\infty} e_N(\alpha)$ *and* $\lim_{N\to+\infty} e^{\text{per}}_{N,L,w}(\alpha)$ *exist, are continuous, and non-decreasing in* α*. Moreover they are equal,*

$$\lim_{N\to+\infty} e^{\text{per}}_{N,L,w}(\alpha) = \lim_{N\to+\infty} e_N(\alpha). \tag{10}$$

Remark about XORSAT We prove such a theorem for K-XORSAT *with* K *even* in Appendix A. The proof breaks down for K odd, although the result is presumably true in that case also.

Standard methods of statistical mechanics [30] do not allow to prove the existence of the limits because the underlying graphs have expansion properties. When the system is cut in two parts the number of edges in the cut is of the same order as the size of the two parts and is not just a "surface" term. Therefore sub-additivity of the free and ground state energies become non-trivial. However, interpolation methods allow to deal with this issue. The existence of the limit for $\lim_{N\to+\infty} e_N(\alpha)$, as well as the fact that the function is continuous and non-decreasing, is proved for a range of models including the present ones in [18, 19], and it is easy to see that the same sort of proof works for the periodic chain. This proof will not be repeated. In Sect. 5 we provide the proof for the *equality* of the two limits. This is again based on two interpolations which provide upper and lower bounds. Note that concentration of the ground state and free energies is also implied by standard arguments not discussed here.[3]

We are interested in the thermodynamic limit

$$\lim_{\text{therm}} \equiv \lim_{L\to+\infty} \lim_{N\to+\infty}$$

for the open chain, which captures the regime of a long one-dimensional coupled-CSP. From Theorems 1 and 2 we deduce that

$$\lim_{\text{therm}} e_{N,L,w}(\alpha) = \lim_{\text{therm}} e^{\text{per}}_{N,L,w}(\alpha) = \lim_{N\to+\infty} e_N(\alpha). \tag{11}$$

Since the energy functions are non-decreasing we can define a natural "static phase transition" threshold as follows.

Definition 1 (Static phase transition threshold) We define

$$\alpha_s = \sup\Big\{\alpha \Big| \lim_{N\to+\infty} e_N(\alpha) = 0\Big\}, \tag{12}$$

and

$$\alpha_{s,L,w} = \sup\Big\{\alpha \Big| \lim_{N\to+\infty} e_{N,L,w}(\alpha) = 0\Big\}. \tag{13}$$

Because of (11) we have

$$\begin{aligned}\alpha_s &= \sup\Big\{\alpha \Big| \lim_{N\to+\infty} e_N(\alpha) = 0\Big\}\\ &= \sup\Big\{\alpha \Big| \lim_{\text{therm}} e^{\text{per}}_{N,L,w}(\alpha) = 0\Big\}\\ &= \sup\Big\{\alpha \Big| \lim_{\text{therm}} e_{N,L,w}(\alpha) = 0\Big\}\end{aligned} \tag{14}$$

Let us now show that $\alpha_s = \lim_{L\to+\infty} \alpha_{s,L,w}$. By using the right-hand inequality in (9) and (10), we have $\lim_{N\to+\infty} e_{N,L,w}(\alpha) \le \lim_{N\to+\infty} e_N(\alpha)$, from which we deduce $\alpha_s \le \liminf_{L\to+\infty} \alpha_{s,L,w}$. Also note that (14) implies $\alpha_s \ge \limsup_{L\to+\infty} \alpha_{s,L,w}$. Indeed if this was not true then one could find α_* and a sequence $L_n \uparrow +\infty$ such that $\alpha_s < \alpha_* < \alpha_{s,L_n,w}$ for n large enough; but then $\lim_{N\to+\infty} e_{N,L_n,w}(\alpha_*) = 0$ and thus $\lim_{n\to+\infty} \lim_{N\to+\infty} e_{N,L_n,w}(\alpha_*) = 0$ which, from (14), would mean $\alpha_* \le \alpha_s$; a contradiction.

The definition of α_s implies that, for a given instance, when $\alpha < \alpha_s$ (resp. $\alpha > \alpha_s$) the number of unsatisfied constraints is $o(N)$ (resp. $O(N)$) with high probability. However it is not known how to automatically conclude that a fixed instance is SAT (resp. UNSAT) with high probability when $\alpha < \alpha_s$ (resp. $\alpha > \alpha_s$).

[3] However concentration of the number of solutions in the SAT phase is more subtle see [29].

Remark about finite temperatures The theorems of this subsection have finite temperature analogs presented in Appendix A. As explained in Sect. 6 these suggest that the condensation threshold obeys $\lim_{L\to+\infty}\alpha_{c,L,w}=\alpha_c$.

2.5 Zero Temperature Cavity Method and Survey Propagation Formalism

We briefly summarize the simplest form of the cavity method and survey propagation equations for the coupled-CSP. More details on the formalism are presented in Appendix B. When the graph instance is a *tree*, the minimization of (3) can be carried out exactly. This leads to an expression for $\min_{\underline{x}}\mathcal{H}_{\rm cou}(\underline{x})$ in terms of energy-cost messages $E_{iu\to cz}(x_{iu})$ and $\hat{E}_{cz\to iu}(x_{iu})$ that satisfy the standard min-sum equations (see Eqs. (140) and (141)). These messages are normalized so that $\min_{x_{iu}}E_{iu\to cz}(x_{iu})=\min_{x_{iu}}\hat{E}_{cz\to iu}(x_{iu})=0$ and they take values in $\{0,1\}$. They may be interpreted as warning messages. Roughly speaking, nodes inform each other on the most favorable values that the variable x_{iu} should take in order to avoid energy costs. The ground state energy (on the tree) is given by the Bethe energy functional $\mathcal{E}[\{E_{iu\to cz}(.),\hat{E}_{cz\to iu}(.)\}]$ (see Eq. (143)). For a *general graph instance* one considers the Bethe energy functional (143) as an "effective Hamiltonian" and studies the statistical mechanics of this effective system. The min-sum equations are the stationary point equations of this functional and the set of solutions $\{E_{iu\to cz}(.),\hat{E}_{cz\to iu}(.)\}$ characterize the *state* of the system.

It turns out that the min-sum equations may have exponentially many (in system size) solutions with infinitesimal Bethe energy per node as $N\to+\infty$. A solution $\{E^{(p)}_{iu\to cz}(.),E^{(p)}_{cz\to iu}(.)\}$ with infinitesimal Bethe energy defines a *pure Bethe state*[4] denoted by the superscript (p). We define the average *zero-energy complexity* as

$$\Sigma_{L,w}(\alpha)=\lim_{\epsilon\to0}\lim_{N\to+\infty}\frac{1}{NL}\mathbb{E}\left[\ln\left(\text{number of states } p \text{ with } \frac{\mathcal{E}^{(p)}}{N}=\epsilon\right)\right]. \tag{15}$$

This quantity counts the number of pure Bethe states. The typical behavior of the complexity as a function of α is as follows. Below an *SP threshold* it vanishes, then jumps to a positive value and decreases until it becomes zero at the static phase transition threshold (and formally negative above). It therefore allows to compute

$$\alpha_{{\rm SP},L,w}=\inf\{\alpha\,|\,\Sigma_{L,w}(\alpha)>0\}, \tag{16}$$

$$\alpha_{s,L,w}=\sup\{\alpha\,|\,\Sigma_{L,w}(\alpha)>0\}. \tag{17}$$

Within the formalism of the cavity method the static phase transition thresholds defined according to the energy (12) and complexity (17) coincide.

The complexity is the Boltzmann entropy (on the zero energy shell) of the effective statistical mechanical problem with Hamiltonian $\mathcal{E}[\{E_{iu\to cz}(.),\hat{E}_{cz\to iu}(.)\}]$. It turns out that this can be computed, thanks to an effective partition function on the same sparse graph instance, again within a message passing formalism. In this context messages are called *surveys*. They count the fraction of pure Bethe states with given warning messages. Surveys $Q_{iu\to cz}(E_{iu\to cz}(.))$ and $\hat{Q}_{cz\to iu}(\hat{E}_{cz\to iu}(.))$ are exchanged between variable and constraint nodes according to survey propagation equations (see (148) and (149)). The average complexity (15) can be computed by a Bethe type formula for the entropy of the effective model.

[4]We adopt this terminology to make a distinction with the mathematically precise notion of *pure state* for usual Ising models [30].

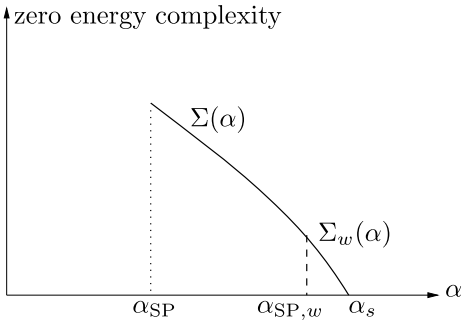

Fig. 2 Complexity of the individual ensemble $\Sigma(\alpha)$ (i.e. $L = w = 1$) and limiting complexity $\Sigma_w(\alpha)$ of the coupled ensemble for $L \to +\infty$. We have $\alpha_{{\rm SP},w} \to \alpha_s$ as $w \to +\infty$

The survey propagation equations (148), (149) allow to compute the distribution over pure Bethe states, of the vectors $(\hat{E}_{cz\to iu}(x_{iu}), x_{iu} \in \mathcal{X})$. These are $|\mathcal{X}|$-component vectors with components in $\{0, 1\}$. Thus the surveys are supported on an alphabet of size at most $2^{|\mathcal{X}|}$. Often the effective size of the alphabet is smaller (it is $|\mathcal{X}| + 1$ in the specific problems considered here) because the warning propagation equations (140), (141) restrict the possible values of $(\hat{E}_{cz\to iu}(x_{iu}), x_{iu} \in \mathcal{X})$. This simplification is used for each model separately in the next sections.

Let us summarize the main observations that follow from the detailed analysis in Sects. 3 and 4. As $L \to +\infty$, we find that the complexity curves $\Sigma_{L,w}(\alpha)$ supported on the interval $[\alpha_{{\rm SP},L,w}, \alpha_{s,L,w}]$ converge to a limiting curve $\Sigma_w(\alpha)$ supported on the limiting interval $[\alpha_{{\rm SP},w}, \alpha_s]$. Moreover, on this later interval, $\Sigma_w(\alpha)$ coincides with the complexity $\Sigma(\alpha)$ of the individual system ($L = w = 1$). This is illustrated on Fig. 2. We observe that $\alpha_{s,L,w}$ tends to α_s from above. Also for moderate L one generally has $\alpha_{{\rm SP},L,w} > \alpha_s$, but this inequality is reversed for L large enough, and $\lim_{L\to+\infty} \alpha_{{\rm SP},L,w} = \alpha_{{\rm SP},w} < \alpha_s$.

We observe the threshold saturation, namely $\lim_{w\to+\infty} \alpha_{{\rm SP},w} \uparrow \alpha_s$. In fact we expect (from [6]) that the gap $|\alpha_{{\rm SP},w} - \alpha_s|$ is exponentially small in w (K fixed) but this is hard to assess numerically. One also observes that for w fixed the gap increases with increasing K.

We point out that the complexity of the chain with periodic boundary conditions converges to that of the individual system in the infinite length limit. In other words there is no threshold saturation as long as the boundary conditions are periodic. This is easily understood by realizing that the survey propagation equations are purely local and have a translation invariant solution when the boundary conditions are periodic.

Finally, let us mention that we observe similar features for the *entropic complexity* curve. In this case α_d plays the role of $\alpha_{\rm SP}$ and α_c that of α_s. We have $\alpha_{d,w} \to \alpha_c$. In particular, $\lim_{L\to+\infty} \alpha_{c,L,w} = \alpha_c$ and $\lim_{w\to+\infty} \lim_{L\to+\infty} \alpha_{d,L,w} = \alpha_c$ (see Sect. 6).

3 Coupled K-SAT Problem

3.1 Numerical Implementation

We begin with a convenient parametrization of the messages (see e.g. [12]). Since $\mathcal{X} = \{0, 1\}$, the warning (energy costs) messages are two-component vectors $(E_{iu\to cz}(0), E_{iu\to cz}(1))$ and $(\hat{E}_{cz\to iu}(0), \hat{E}_{cz\to iu}(1))$ which take three possible values $(0, 1)$, $(1, 0)$ and $(0, 0)$. Warning $(0, 1)$ means that x_{iu} should take the value 0, warning $(1, 0)$ means

that x_{iu} should take value 1, and warning $(0,0)$ means that x_{iu} is free to take any value. Messages from variables to constraints can be conveniently parametrized as follows,

$$Q^S_{iu\to cz} \equiv \begin{cases} Q_{iu\to cz}(0,1) & \text{if } x_{iu} \text{ is negated in } cz, \\ Q_{iu\to cz}(1,0) & \text{if } x_{iu} \text{ is not negated in } cz. \end{cases}$$

This is the fraction of pure states for which the variable is forced to satisfy the constraint. Similarly,

$$Q^U_{iu\to cz} \equiv \begin{cases} Q_{iu\to cz}(0,1) & \text{if } x_{iu} \text{ is not negated in } cz, \\ Q_{iu\to cz}(1,0) & \text{if } x_{iu} \text{ is negated in } cz. \end{cases}$$

This is the fraction of pure states for which the variable is forced to unsatisfy the constraint. Note that $Q_{iu\to cz}(0,0) = 1 - Q^S_{iu\to cz} - Q^U_{iu\to cz}$. Let us now parametrize the messages from constraints to variables. If variable x_{iu} enters unnegated in constraint cz, then certainly constraint cz does not force it to take the value 0. Thus $\hat{Q}_{cz\to iu}(0,1) = 0$, and the message can be parametrized by the single number $\hat{Q}_{cz\to iu}(1,0)$. On the other hand, if variable x_{iu} enters negated in constraint cz, then certainly constraint cz does not force it to take the value 1. Thus $\hat{Q}_{cz\to iu}(1,0) = 0$, and again the message can be parametrized by the single number $\hat{Q}_{cz\to iu}(0,1)$. We set

$$\hat{Q}_{cz\to iu} \equiv \begin{cases} \hat{Q}_{cz\to iu}(0,1) & \text{if } x_{iu} \text{ is negated in } cz, \\ \hat{Q}_{cz\to iu}(1,0) & \text{if } x_{iu} \text{ is not negated in } cz. \end{cases}$$

Message $\hat{Q}_{cz\to iu}$ is the fraction of pure states for which cz warns iu to satisfy it. The survey propagation equations (148), (149) then become (recall $d_{\langle bv,iu\rangle} = 1$ (resp. 0) for a dashed (resp. full) edge $\langle bv, iu\rangle$),

$$\hat{Q}_{cz\to iu} = \prod_{jv\in\partial(cz)\setminus iu} Q^U_{jv\to cz}, \tag{18}$$

and

$$Q^S_{iu\to cz} \cong \left\{ \prod_{bv\in\partial(iu)\setminus cz}^{d_{\langle bv,iu\rangle}\neq d_{\langle iu,cz\rangle}} (1-\hat{Q}_{bv\to iu}) \right\} \left\{ 1 - \prod_{bv\in\partial(iu)\setminus cz}^{d_{\langle bv,iu\rangle}= d_{\langle iu,cz\rangle}} (1-\hat{Q}_{bv\to iu}) \right\}, \tag{19}$$

$$Q^U_{iu\to cz} \cong \left\{ \prod_{bv\in\partial(iu)\setminus cz}^{d_{\langle bv,iu\rangle}= d_{\langle iu,cz\rangle}} (1-\hat{Q}_{bv\to iu}) \right\} \left\{ 1 - \prod_{bv\in\partial(iu)\setminus cz}^{d_{\langle bv,iu\rangle}\neq d_{\langle iu,cz\rangle}} (1-\hat{Q}_{bv\to iu}) \right\}, \tag{20}$$

where $\cong$ means that the r.h.s. has to be normalized to one. Define

$$Q^+_{iu\to cz} = \prod_{bv\in\partial(iu)\setminus cz}^{d_{\langle bv,iu\rangle}= d_{\langle iu,cz\rangle}} (1-\hat{Q}_{bv\to iu}), \tag{21}$$

$$Q^-_{iu\to cz} = \prod_{bv\in\partial(iu)\setminus cz}^{d_{\langle bv,iu\rangle}\neq d_{\langle iu,cz\rangle}} (1-\hat{Q}_{bv\to iu}). \tag{22}$$

Then using (18) and the normalized form of (20)

$$\hat{Q}_{cz\to iu} = \prod_{jv\in\partial(cz)\setminus iu} \frac{Q^+_{jv\to cz}(1-Q^-_{jv\to cz})}{Q^+_{jv\to cz} + Q^-_{jv\to cz} - Q^+_{jv\to cz}Q^-_{jv\to cz}}. \tag{23}$$

We will work with the set of SP equations (21), (22), (23). The complexity becomes

$$\Sigma_{L,w}(\alpha) = \frac{1}{NL}\mathbb{E}\Big[\sum_{cz}\Sigma_{cz} + \sum_{iz}\Sigma_{iz} - \sum_{\langle cz,iu\rangle}\Sigma_{cz,iu}\Big], \tag{24}$$

with

$$\Sigma_{cz} = \ln\Big\{\prod_{iu\in\partial(cz)}\big(Q^{+}_{iu\to cz} + Q^{-}_{iu\to cz} - Q^{+}_{iu\to cz}Q^{-}_{iu\to cz}\big) - \prod_{iu\in\partial(cz)}Q^{+}_{iu\to cz}\big(1-Q^{-}_{iu\to cz}\big)\Big\}, \tag{25}$$

$$\Sigma_{iz} = \ln\Big\{\prod_{bv\in\partial(iz)}^{d_{\langle bv,iz\rangle}=1}(1-\hat{Q}_{bv\to iz}) + \prod_{bv\in\partial(iz)}^{d_{\langle bv,iz\rangle}=0}(1-\hat{Q}_{bv\to iz}) - \prod_{bv\in\partial(iz)}(1-\hat{Q}_{bv\to iz})\Big\}, \tag{26}$$

$$\Sigma_{cz,iu} = \ln\big\{\big(Q^{+}_{iu\to cz} + Q^{-}_{iu\to cz} - Q^{+}_{iu\to cz}Q^{-}_{iu\to cz}\big) - Q^{+}_{iu\to cz}\big(1-Q^{-}_{iu\to cz}\big)\hat{Q}_{cz\to iu}\big\}. \tag{27}$$

The set of SP equations (21), (22), (23) is solved under the following assumptions. We treat the set of messages emanating from a constraint at position z, namely $\hat{Q}_{cz\to iu}$ for $u = z,\dots,z+w-1$, as i.i.d. copies of a r.v. $\hat{Q}_z$ depending only on the position z. Similarly we treat the messages emanating from a variable node at position u, namely $Q^{\pm}_{iu\to cz}$ for $z = u-w+1,\dots,u$, as i.i.d. copies of a r.v. $Q^{\pm}_{u}$. Now, fix a position z and pick p, q two independent Poisson($\frac{\alpha K}{2}$) integers. Pick $k_1,\dots,k_{p+q}$ independently uniformly in $\{0,\dots,w-1\}$. Similarly, pick $l_1,\dots,l_{K-1}$ independently uniformly in $\{0,\dots,w-1\}$. Under our assumptions the SP equations become[5]

$$Q^{+}_{z} = \prod_{i=1}^{p}\big(1-\hat{Q}^{(i)}_{z-k_i}\big), \tag{28}$$

$$Q^{-}_{z} = \prod_{i=p+1}^{p+q}\big(1-\hat{Q}^{(i)}_{z-k_i}\big), \tag{29}$$

and

$$\hat{Q}_z = \prod_{i=1}^{K-1}\frac{Q^{+(i)}_{z+l_i}\big(1-Q^{-(i)}_{z+l_i}\big)}{Q^{+(i)}_{z+l_i} + Q^{-(i)}_{z+l_i} - Q^{+(i)}_{z+l_i}Q^{-(i)}_{z+l_i}}. \tag{30}$$

The boundary conditions can be taken into account by setting $\hat{Q}_z = 0$ for $z \le -\frac{L}{2}$, $z > \frac{L}{2}$. These equations are solved by the standard method of population dynamics. It is then possible to compute the average complexity from

$$\Sigma_{L,w}(\alpha) = \frac{1}{L}\sum_{z=-\frac{L}{2}+1}^{\frac{L}{2}}\big(\alpha\mathbb{E}\big[\Sigma^{\text{cons}}_{z}\big] + \mathbb{E}\big[\Sigma^{\text{var}}_{z}\big] - \alpha K\mathbb{E}\big[\Sigma^{\text{edge}}_{z}\big]\big), \tag{31}$$

where

$$\Sigma^{\text{cons}}_{z} = \ln\Big\{\prod_{i=1}^{K}\big(Q^{+(i)}_{z+l_i} + Q^{-(i)}_{z+l_i} - Q^{+(i)}_{z+l_i}Q^{-(i)}_{z+l_i}\big) - \prod_{i=1}^{K}Q^{+(i)}_{z+l_i}\big(1-Q^{-(i)}_{z+l_i}\big)\Big\}, \tag{32}$$

$$\Sigma^{\text{var}}_{z} = \ln\Big\{\prod_{i}^{p}\big(1-\hat{Q}^{(i)}_{z-k_i}\big) + \prod_{i=p+1}^{p+q}\big(1-\hat{Q}^{(i)}_{z-k_i}\big) - \prod_{i=1}^{p+q}\big(1-\hat{Q}^{(i)}_{z-k_i}\big)\Big\}, \tag{33}$$

[5] In (28), (29), (30) equalities mean that the r.v. have the same distribution.

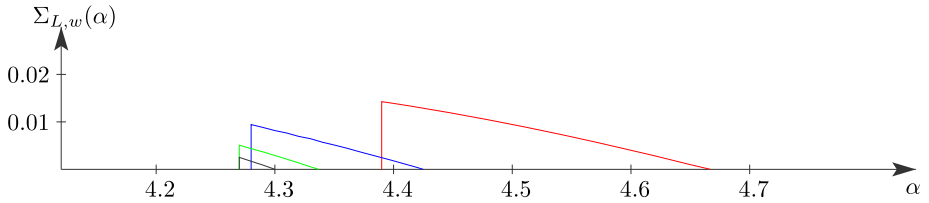

Fig. 3 Average complexity versus α for the $[1000, 3, \alpha, 3, L]$ ensembles with $L = 10$ (*rightmost curve*), 20, 40, 80 (*leftmost curve*). Values of the corresponding thresholds are given in Table 1

Table 1 SP and static phase transition thresholds of the $[1000, 3, \alpha, 3, L]$ ensembles

Individual	α_{SP}	α_s
$L = 1$	3.927	4.267
Coupled	$\alpha_{\mathrm{SP},L,3}$	$\alpha_{s,L,3}$
$L = 10$	4.386	4.663
$L = 20$	4.274	4.425
$L = 40$	4.269	4.335
$L = 80$	4.268	4.301
$L = 160$	4.267	4.284

$$\Sigma_z^{\mathrm{edge}} = \ln\left\{\left(Q_{z+k}^{+} + Q_{z+k}^{-} - Q_{z+k}^{+}Q_{z+k}^{-}\right) - Q_{z+k}^{+}\left(1 - Q_{z+k}^{-}\right)\hat{Q}_z\right\}. \tag{34}$$

Figure 3 shows the average complexity for the regime $N \gg L \gg w$, for $K = 3$ and $w = 3$. We find it is positive in an interval $[\alpha_{\mathrm{SP},L,w}, \alpha_{s,L,w}]$ whose size shrinks as L increases. The two end points of this interval are given in Table 1 (corresponding to Fig. 3). Let us comment on the numerical findings.

First, we observe that $\alpha_{\mathrm{SP},L,w}$ approaches α_s as L increases. It is hard to compute more than three digits with population dynamics experiments but we expect that a small difference should remain between $\lim_{L\to\infty} \alpha_{\mathrm{SP},L,w}$ and α_s. This difference should decrease very fast as w grows, and in fact for $w = 3$ one does not see it in the first three digits. For the Curie-Weiss chain [6] this difference has been analytically calculated to be exponentially small[6] in w. For the paradigmatic spatially coupled LDPC codes the difference appears only in the sixth decimal figure when state of the art density evolution numerics is used [2].

Second, we observe that $\alpha_{s,L,w}$ decreases as L increases. An extrapolation of the values suggests that as L grows larger (i.e., $L = 320, 640, \ldots$) $\alpha_{s,L,w}$ should come closer to α_s. However these lengths become prohibitive for population dynamics. As discussed in Sect. 2.4 we know on theoretical grounds that $\lim_{L\to+\infty} \alpha_{s,L,w} = \alpha_s$ is true for all w.

For moderate values of L we have $\alpha_s < \alpha_{\mathrm{SP},L,w}$. However since $\alpha_{\mathrm{SP},L,w} < \alpha_{s,L,w}$ and $\lim_{L\to+\infty} \alpha_{s,L,w} = \alpha_s$, for L large enough and fixed w we necessarily have $\alpha_{\mathrm{SP},L,w} < \alpha_s$. This turns out to be difficult to observe within population dynamics experiments, but can be checked in the large K limit.

[6] The calculation involves a non-perturbative calculation of potential energy barriers in terms of a deformation parameter $\frac{1}{w}$ when going from a continuum to a discrete model.

3.2 Survey Propagation for Large K

For large K one can derive approximations of the survey propagation equations that lend themselves to more explicit analysis [41]. We will not attempt to control the error terms, but it is known for the individual system that the approximations are excellent already for $K \geq 5$. We can check numerically that this is also the case for the coupled-CSP.

3.2.1 Fixed Point Equations

Following [41], we introduce entropic random variables

$$\hat{q}_z = -\ln(1-\hat{Q}_z), \qquad q_z^{\pm} = -\ln Q_z^{\pm}. \tag{35}$$

From (28), (29) and (30) we obtain

$$q_z^{+} = \sum_{i=1}^{p} \hat{q}_{z-k_i}^{(i)}, \qquad q_z^{-} = \sum_{i=p+1}^{p+q} \hat{q}_{z-k_i}^{(i)}, \tag{36}$$

and

$$\hat{q}_z = -\ln\left\{1 - \prod_{i=1}^{K-1} \frac{e^{q_{z+l_i}^{-(i)}} - 1}{e^{q_{z+l_i}^{-(i)}} + e^{q_{z+l_i}^{+(i)}} - 1}\right\}, \tag{37}$$

we set

$$\mathbb{E}\big[q_z^{\pm}\big] = x_z^{\pm} \quad \text{and} \quad \mathbb{E}[\hat{q}_z] = y_z, \tag{38}$$

for the averages over the graph ensemble. The number of i.i.d. random variables in (36) is a Poisson($\frac{\alpha K}{2}$) integer. Therefore we assume that for large K the r.v. $q_z^{\pm}$ are self-averaging. It is reasonable to expect that they can be replaced by their expectation in (37) and that hence $\hat{q}_z$ is also self-averaging. This implies a closed set of equations for the expected values of messages,

$$\begin{cases} x_z^{\pm} \approx \frac{\alpha K}{2w} \sum_{k=0}^{w-1} y_{z-k}, \\ y_z \approx -\sum_{k_1,\ldots,k_{K-1}=0}^{w-1} \frac{1}{w^{K-1}} \ln\{1 - \prod_{i=1}^{K-1} \frac{e^{x_{z+k_i}^{-}} - 1}{e^{x_{z+k_i}^{-}} + e^{x_{z+k_i}^{+}} - 1}\}. \end{cases} \tag{39}$$

We further approximate (39). A self-consistent check with the final solution shows that $x^{\pm} = O(K)$ and hence the product in the log is $O(2^{-K})$. Linearizing the logarithm yields

$$y_z \approx \sum_{k_1,\ldots,k_{K-1}=0}^{w-1} \frac{1}{w^{K-1}} \prod_{i=1}^{K-1} \frac{e^{x_{z+k_i}^{-}} - 1}{2e^{x_{z+k_i}^{-}} - 1} = \left\{\frac{1}{w} \sum_{k=0}^{w-1} \frac{e^{x_{z+k}^{-}} - 1}{2e^{x_{z+k}^{-}} - 1}\right\}^{K-1}. \tag{40}$$

It is convenient to introduce the rescaled parameters

$$\hat{\alpha} = 2^{-K}\alpha, \qquad \varphi_z = 2^{K-1}\hat{\alpha} K y_z. \tag{41}$$

From (35) we see φ_z is a measure of the average (over the graph ensemble) probability (over pure states) that constraints at position z send warning messages. From now on we write x_z instead of $x_z^{\pm}$. The fixed point equations become

$$\begin{cases} x_z \approx \frac{1}{w} \sum_{k=0}^{w-1} \varphi_{z-k}, \\ \varphi_z \approx \hat{\alpha} K \{\frac{1}{w} \sum_{l=0}^{w-1} \frac{e^{x_{z+l}} - 1}{e^{x_{z+l}} - \frac{1}{2}}\}^{K-1}. \end{cases} \tag{42}$$

Hence, the profile $\{\varphi_z\}$ satisfies

$$\varphi_z \approx \hat{\alpha} K \left\{ \frac{1}{w} \sum_{k=0}^{w-1} \frac{e^{\frac{1}{w}\sum_{l=0}^{w-1}\varphi_{z-l+k}} - 1}{e^{\frac{1}{w}\sum_{l=0}^{w-1}\varphi_{z-l+k}} - \frac{1}{2}} \right\}^{K-1}. \tag{43}$$

These equations have to be supplemented with the boundary condition $\varphi_z = 0$ for $z \le -\frac{L}{2}$ and $z > \frac{L}{2}$.

3.2.2 The Average Complexity

Let us now express the complexity in terms of the fixed point profile. Let us first compute the contributions of variable and constraint nodes, and of edges.

Contribution of Variable Nodes From (33), (35) and (38)

$$\Sigma_z^{\text{var}} = \ln\left\{ e^{-\sum_{i=1}^{p}\hat{q}_{z-k_i}} + e^{-\sum_{i=p+1}^{q}\hat{q}_{z-k_i}} - e^{-\sum_{i=1}^{p+q}\hat{q}_{z-k_i}} \right\}. \tag{44}$$

For K large the sums in the exponentials concentrate on their averages, so that

$$\mathbb{E}\left[\Sigma_z^{\text{var}}\right] \approx \ln\left\{ 2e^{-\frac{\alpha K}{2w}\sum_{k=0}^{w-1} y_{z-k}} - e^{-\frac{\alpha K}{w}\sum_{k=0}^{w-1} y_{z-k}} \right\}. \tag{45}$$

Contribution of Check Nodes From (32), (35) and (38)

$$\begin{aligned}\mathbb{E}\left[\Sigma_z^{\text{cons}}\right] &= \mathbb{E}\left[\ln\left\{ \prod_{i=1}^{K}\left(e^{-q^+_{z+l_i}} + e^{-q^-_{z+l_i}} - e^{-q^+_{z+l_i}-q^-_{z+l_i}}\right) - \prod_{i=1}^{K} e^{-q^+_{z+l_i}}\left(1 - e^{-q^-_{z+l_i}}\right) \right\} \right] \\ &\approx \sum_{l_1,\dots,l_K=0}^{w-1} \frac{1}{w^K} \ln\left\{ \prod_{i=1}^{K}\left(2e^{-x^-_{z+l_i}} - e^{-2x^-_{z+l_i}}\right) - \prod_{i=1}^{K} e^{-x^-_{z+l_i}}\left(1 - e^{-x^-_{z+l_i}}\right) \right\}. \end{aligned} \tag{46}$$

Factoring the first product out of the log we get

$$\mathbb{E}\left[\Sigma_z^{\text{cons}}\right] \approx \frac{K}{w}\sum_{l=0}^{w-1} \ln\left\{2e^{-x^-_{z+l}} - e^{-2x^-_{z+l}}\right\} + \sum_{l_1,\dots,l_K=0}^{w-1} \frac{1}{w^K} \ln\left\{ 1 - \prod_{i=1}^{K} \frac{1 - e^{-x^-_{z+l_i}}}{2 - e^{-x^-_{z+l}}} \right\}. \tag{47}$$

Since the ratio in the second log is $O(2^{-K})$ we can linearize and obtain

$$\mathbb{E}\left[\Sigma_z^{\text{cons}}\right] \approx \frac{K}{w}\sum_{l=0}^{w-1} \ln\left\{2e^{-x^-_{z+l}} - e^{-2x^-_{z+l}}\right\} - \left\{ \frac{1}{w}\sum_{l=0}^{w-1} \frac{1 - e^{-x^-_{z+l}}}{2 - e^{-x^-_{z+l}}} \right\}^K. \tag{48}$$

Contribution of Edges Similarly from (34), (35), (38) we have

$$\begin{aligned}\mathbb{E}\left[\Sigma_z^{\text{edge}}\right] &= \frac{1}{w}\sum_{l=0}^{w-1} \mathbb{E}\left[\ln\left\{\left(e^{-q^+_{z+l}} + e^{-q^-_{z+l}} - e^{-q^+_{z+l}-q^-_{z+l}}\right) - e^{-q^+_{z+l}}\left(1 - e^{-q^-_{z+l}}\right)\left(1 - e^{-\hat{q}_z}\right)\right\}\right] \\ &\approx \frac{1}{w}\sum_{l=0}^{w-1} \ln\left\{\left(2e^{-x^-_{z+l}} - e^{-2x^-_{z+l}}\right) - e^{-x^-_{z+l}}\left(1 - e^{-x^-_{z+l}}\right)\left(1 - e^{-y_z}\right)\right\}. \end{aligned} \tag{49}$$

Now, using (39) we can express the total average complexity (31) in terms of rescaled variables (41). We find

$$\Sigma_{w,L}(\hat{\alpha}) = \frac{1}{L}\sum_{z=-\frac{L}{2}+1}^{\frac{L}{2}} \sigma_{\hat{\alpha},w,L}(z), \tag{50}$$

with

$$\sigma_{\hat{\alpha},w,L}(z) \approx \ln\left\{2e^{-\sum_{k=0}^{w-1}\varphi_{z-k}} - e^{-\frac{2}{w}\sum_{k=0}^{w-1}\varphi_{z-k}}\right\} - 2^K\hat{\alpha}\left\{\frac{1}{w}\sum_{l=0}^{w-1}\frac{e^{x_{z+l}}-1}{2e^{x_{z+l}}-1}\right\}^K$$
$$-\frac{2^K\hat{\alpha}K}{w}\sum_{l=0}^{w-1}\ln\left\{1-\frac{e^{x_{z+l}}-1}{2e^{x_{z+l}}-1}\left(1-e^{-\frac{\varphi_z}{\hat{\alpha}K2^{K-1}}}\right)\right\}. \tag{51}$$

Within our approximations the third term can be simplified further because $1-e^{-\frac{\varphi_z}{K2^{K-1}}} = O(2^{-K})$ and we may linearize the log. Thus the second line in (51) can be replaced by

$$2\varphi_z\frac{1}{w}\sum_{l=0}^{w-1}\left\{\frac{e^{x_{z+l}}-1}{2e^{x_{z+l}}-1}\right\}. \tag{52}$$

The complexity (50) can be viewed as a functional of the profiles $\{x_z, \varphi_z\}$ with boundary condition $\varphi_z = 0$ for $z \le -\frac{L}{2}$ and $z > \frac{L}{2}$. One can check that the stationary points of this functional are given by the fixed point equations (42).

3.3 Solutions for Large K

We use the notation $f \doteq g$ to mean that $\lim_{K\to+\infty}\frac{f}{g} = 1$. The large K results for the individual system [41] are recovered by setting $L = w = 1$, in which case the fixed point equations (43) reduces to

$$\varphi \approx \hat{\alpha}K\left\{\frac{e^{\varphi}-1}{e^{\varphi}-\frac{1}{2}}\right\}^{K-1}. \tag{53}$$

One may easily check that this is the stationary point equation for the complexity (50) as a function of φ (and α fixed),

$$\Sigma_{1,1}(\hat{\alpha},\varphi) = \ln\left\{2e^{-\varphi} - e^{-2\varphi}\right\} - 2K\hat{\alpha}\left\{\frac{e^{\varphi}-1}{2e^{\varphi}-1}\right\}^K + \varphi\left\{\frac{e^{\varphi}-1}{2e^{\varphi}-1}\right\}. \tag{54}$$

Thus, fixed points of (53) are stationary points of (54): stable fixed points correspond to minima and unstable ones to maxima.

The curve $\hat{\alpha}(\varphi)$ is shown as the dotted curve in Fig. 5. This function is convex and has a unique minimum at $\varphi_{\rm SP} \doteq \ln(\frac{1}{2}K\ln K)$ and $\hat{\alpha}(\varphi_{\rm SP}) \equiv \hat{\alpha}_{\rm SP} \doteq \frac{\ln K}{K}$. Near this minimum we have $\hat{\alpha}(\varphi) \approx (\frac{\varphi-\varphi_{\rm SP}}{\gamma_{\rm SP}})^2$, $\gamma_{\rm SP} \doteq \frac{4}{3}\frac{K}{\ln K}$. For $\varphi \gg \varphi_{\rm SP}$ we have $\hat{\alpha}(\varphi) = \frac{1}{K}(\varphi-\varphi_{\rm SP})$ and for $0 < \varphi \ll \varphi_{\rm SP}$ we have $\hat{\alpha}(\varphi) = \frac{1}{\varphi}$. Therefore the trivial fixed point $\varphi = 0$ is unique for $\hat{\alpha} < \hat{\alpha}_{\rm SP}$, and there are two extra non-trivial fixed points for $\hat{\alpha} > \hat{\alpha}_{\rm SP}$. Only one of them is stable and forms the branch $\varphi_{\rm mst} \approx K\hat{\alpha} + \varphi_{\rm SP}$ for $\varphi \gg \varphi_{\rm SP}$.

For $\hat{\alpha} < \hat{\alpha}_{\rm SP}$, the function (54) has a unique minimum at $\varphi = 0$. For $\hat{\alpha} > \hat{\alpha}_{\rm SP}$ a second metastable minimum appears at $\varphi_{\rm mst} \approx K\hat{\alpha} + \varphi_{\rm SP}$. At this minimum we find $\Sigma_{1,1}(\hat{\alpha}, \varphi_{\rm mst}) \doteq \ln 2 - \hat{\alpha}$ which counts the number of clusters as long as it is positive. Summarizing, the complexity vanishes for $\hat{\alpha} < \hat{\alpha}_{\rm SP}$, and equals $(\ln 2 - \hat{\alpha})$ for $\hat{\alpha} \in [\hat{\alpha}_{\rm SP}, \ln 2]$. In particular the static phase transition threshold is $\hat{\alpha}_s \doteq \ln 2$. Beyond the static phase transition threshold the complexity is negative and looses its meaning (one has to modify the SP formalism used here). Higher order corrections can be computed in powers of 2^{-K}, see [41].

Let us now discuss the coupled case. The picture which emerges is similar to the one for the much simpler Curie-Weiss Chain model [6] and coupled LDPC codes over the binary erasure channel [2]. Before discussing the numerical results we wish to give a heuristic

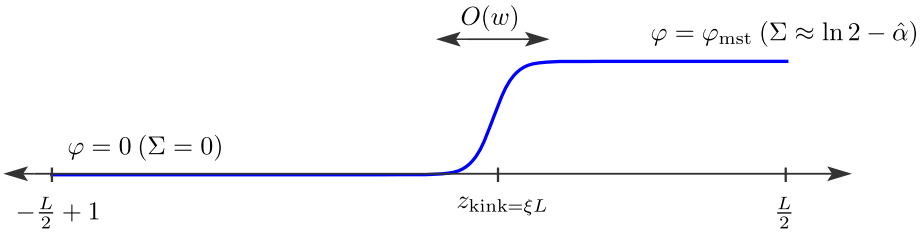

Fig. 4 An illustrative picture of a kink-like ansatz $\{\varphi_z\}_{z=-\frac{L}{2}+1}^{\frac{L}{2}}$ for a solution of (43). At the *right end*, the kink converges to the value $\varphi = \varphi_{\rm st}$ (with corresponding complexity $\Sigma \approx \ln 2 - \hat{\alpha}$) and at the *left end* it converges to $\varphi = 0$ (with $\Sigma = 0$). The transition region of size $O(w)$ which is centered at $z = z_{\rm kink}$

argument that "explains" why threshold saturation occurs. The argument can presumably be turned into a rigorous proof using the methods in [2] for LDPC codes on the binary erasure channel, or more general methods developed in [42].

For the sake of the argument suppose that we fix $\hat{\alpha} > \hat{\alpha}_{\rm SP}$ and that we look for profile solutions of (43), on an infinite chain $L \to +\infty$, that interpolate between the (asymmetric) boundary conditions $\varphi_z = 0$, $z \to -\infty$ and $\varphi_z \to \varphi_{\rm mst}$, $z \to +\infty$. We take as an ansatz, a kink approaching its asymptotic values (at the two ends) fast enough, with a transition region localized in a region of size $O(w)$ centered at a position $z_{\rm kink} = \xi L$ ($|\xi| \le 1/2$). Figure 4 gives an illustrative picture of the kink profile. We have

$$\bar{\varphi} \equiv \frac{1}{L} \sum_{z=-\frac{L}{2}+1}^{\frac{L}{2}} \varphi_z \approx \frac{1}{L}\left(\frac{L}{2} - \xi L\right)\varphi_{\rm mst}. \tag{55}$$

Also, it is easy to see that the associated complexity as a function of ξ, or equivalently $\bar{\varphi}$, is approximately given by a convex combination of the two minima of $\Sigma_{1,1}(\alpha, \varphi)$ (given in (54)) which correspond to the two points $\varphi = 0$ (with $\Sigma = 0$) and $\varphi = \varphi_{\rm st}$ (with $\Sigma \approx \ln 2 - \hat{\alpha}$). More precisely,

$$\begin{aligned}\Sigma_{\rm kink}(\xi) &\approx \frac{1}{L}\left[\left(\frac{L}{2} + \xi L\right) \times 0 + \left(\frac{L}{2} - \xi L\right) \times (\ln 2 - \hat{\alpha})\right] \\ &\approx \frac{\bar{\varphi}}{\varphi_{\rm mst}}(\ln 2 - \hat{\alpha}).\end{aligned}$$

When $\hat{\alpha} < \hat{\alpha}_s$, the minimum is at $\xi = \frac{1}{2}$ ($\bar{\varphi} = 0$). This means that the kink center will form a traveling wave through the chain, and reach its unique stable location at the right end. On the other hand when $\hat{\alpha} > \hat{\alpha}_s$ the minimum is at $\xi = -\frac{1}{2}$ ($\bar{\varphi} = \varphi_{\rm mst}$) and the kink will travel towards the left to reach its stable location. Within the present approximation, for $\hat{\alpha} = \hat{\alpha}_s$ any position along the chain is stable for the kink center.

Summarizing, this heuristic argument suggests that for $\hat{\alpha} < \hat{\alpha}_s$ the fixed point equations (43) only have the trivial solution $\{\varphi_z = 0\}$, while for $\hat{\alpha} > \hat{\alpha}_s$ the only solution is $\{\varphi_z = \varphi_{\rm mst}\}$. This means that the SP threshold coincides with $\hat{\alpha}_s$. Here, ξ has been treated as a continuous variable, which is expected to be valid only in a limit of large w. For large but finite w there will subsist a small gap between the SP and static thresholds, and for $\hat{\alpha}$ fixed in this gap only a discrete set of positions for the kink are stable. The number of such stable positions is roughly equal to $2L$.

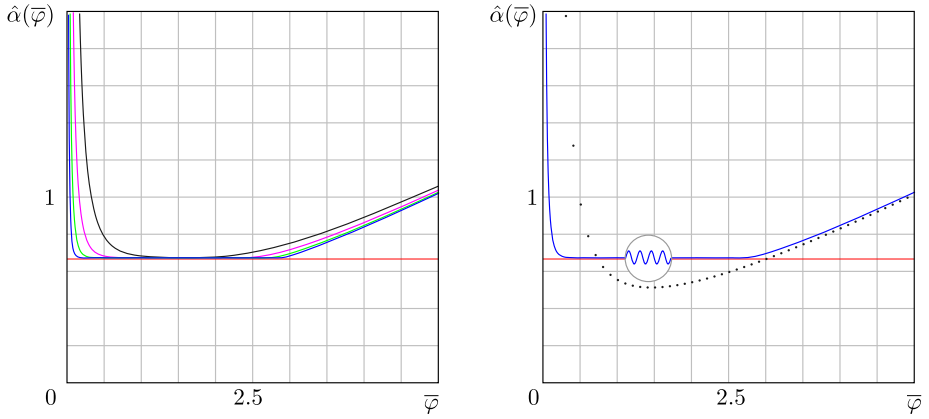

Fig. 5 *Left*: sequence of van der Waals curves $\hat{\alpha}(\bar{\varphi})$, for $K = 5$, $w = 3$ and $L = 10, 20, 40, 80$ (*top* to *bottom*). For $\bar{\varphi} \in [\varphi_{\text{mst}}, +\infty]$ they converge to the individual system curve. *Right*: a magnification of the plateau region for $K = 5$, $w = 3$ and $L = 40$ shows the fine structure. The *dotted line* is the curve for the individual system and the *horizontal line* shows the static phase transition threshold $\hat{\alpha}_s = 0.666$

Table 2 SP thresholds of the individual ($L = w = 1$) and coupled ensembles ($L = 80$, $w = 3, 5, 7$) are found from the van der Waals curves. For $K = 10$ we clearly see that the SP threshold saturates to $\hat{\alpha}_s$ from below as w increases

K	5	7	10
$\hat{\alpha}_s$	0.666	0.686	0.692
$\hat{\alpha}_{\text{SP}}$	0.513	0.449	0.370
$\hat{\alpha}_{\text{SP},80,3}$	0.672	0.682	0.651
$\hat{\alpha}_{\text{SP},80,5}$	0.672	0.688	0.691
$\hat{\alpha}_{\text{SP},80,7}$	0.672	0.688	0.692

We have solved (43) numerically with *symmetric* boundary conditions $\varphi_z = 0$, $z \leq -\frac{L}{2}$, $z > \frac{L}{2}$ and fixed $\bar{\varphi} \equiv \frac{1}{L}\sum_{z=-\frac{L}{2}}^{\frac{L}{2}} \varphi_z$. In order to find a solution for *all* values of $\bar{\varphi}$ we have to let $\hat{\alpha}$ vary slightly. In other words we find a solution $(\hat{\alpha}(\bar{\varphi}); \{\varphi_z(\bar{\varphi})\})$ that is parametrized by $\bar{\varphi}$. Define the *van der Waals curve* (Fig. 5) as the function $\hat{\alpha}(\bar{\varphi})$. The minimum of the van der Waals curve yields (as for the individual system) the SP threshold $\alpha_{\text{SP},w,L}$ (see Table 2 for numerical values).

As L increases, the curves develop a plateau at height $\approx \hat{\alpha}_s$ for the interval $\bar{\varphi} \in [0, \varphi_{\text{mst}}]$. Moreover they converge to the van der Waals curve of the individual system for $\bar{\varphi} \in [\varphi_{\text{mst}}, +\infty[$, a fact that is consistent with Theorems 1, 2. Precise enough numerics show that as long as w is finite the curves display a fine structure in the plateau interval: the magnification in Fig. 5 shows wiggles of very small amplitude. We observe that their amplitude decays as w grows and K is fixed (we expect from [6] that this decay is exponential); and grows larger as K increases with w fixed (see Table 2).

Figure 6 illustrates the solutions of the fixed point equations for $\hat{\alpha}$ in the wiggle region for large K. The top curve is the van der Waals curve in the wiggle region. The middle left warning density profile is the fixed point solution corresponding the left point with coordinates $(\bar{\varphi}_l, \hat{\alpha}_l)$. Note that $\hat{\alpha}_l = \hat{\alpha}_{\text{SP},L,w}$. For this point the total average complexity is approximately equal to $\frac{\bar{\varphi}_l}{\varphi_{\text{mst}}}(\hat{\alpha}_s - \hat{\alpha}_l)$. The bottom left curve shows the complexity profile. In the middle

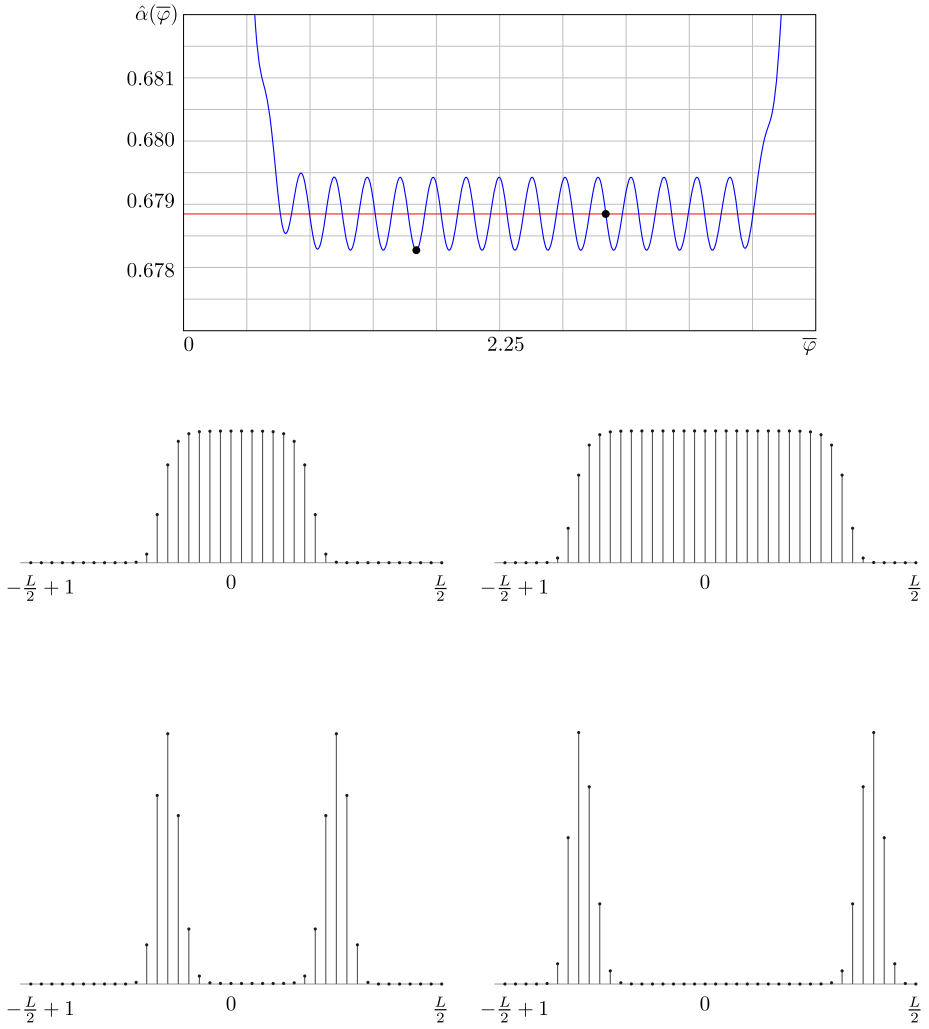

Fig. 6 van der Waals curve in the *wiggle region* for the coupled system (*top*) for $K = 7$, $w = 4$ and $L = 40$. The *horizontal line* is at the static phase transition threshold. The *left point* $(\overline{\varphi}_l, \hat{\alpha}_l) = (1.657, 0.678274)$ corresponds to the warning (*middle left*) and complexity (*bottom left*) profiles. In the latter the height of the middle part is $\hat{\alpha}_s - \hat{\alpha}_l \approx 0.010$. The *right point* $(\overline{\varphi}_r, \hat{\alpha}_r) = (3.00585, 0.688847)$ corresponds to the warning and complexity profiles *on the right*

part, the height of this profile is approximately $(\hat{\alpha}_s - \hat{\alpha}_l) \approx 0.010$. Consider now the point on the right with coordinates $(\overline{\varphi}_r, \hat{\alpha}_r)$. Note that we take this point very close to the static phase transition threshold $\hat{\alpha}_r \approx \hat{\alpha}_s$. As a consequence the total average complexity nearly vanishes. The middle right warning density profile is flat over the whole chain, except near the ends because we enforce the boundary conditions, and the complexity density nearly vanishes except in the transition regions.

4 Coupled Q-Coloring Problem

4.1 Numerical Implementation

First we introduce an adequate parametrization of the messages (see e.g [12]). The warning vectors $(E_{jv\to cz}(1),\dots,E_{jv\to cz}(Q))$ fall in two categories: those that have *exactly one* zero component; and those that have *at least two* zero components. For coloring, Eq. (141) becomes

$$\hat{E}_{cz\to iu}(x_{iu}) = \min_{x_{\partial cz\setminus iu}} \left\{ \mathbb{1}(x_{cz} = x_{jv}) + E_{jv\to cz}(x_{jv}) \right\} - \hat{C}_{cz\to iu}. \tag{56}$$

It is easy to see that when $E_{jv\to cz}$ has exactly one zero component, then $\hat{E}_{cz\to iu}$ has exactly one non-zero component. On the other hand, when $E_{jv\to cz}$ has at least two zero components then all components of $\hat{E}_{cz\to iu}$ are zero. Hence, the vector $(\hat{E}_{cz\to iu}(1),\dots,\hat{E}_{cz\to iu}(Q))$ can take only $Q+1$ possible values which are the $(0,\dots,0)\equiv *$ vector and the Q canonical basis vectors $(1,0,\dots,0)\equiv 1$, $(0,1,0,\dots,0)\equiv 2,\dots,(0,\dots,1)\equiv Q$. The interpretation is clear: a warning vector $\in\{1,\dots,Q\}$ forces the variable to choose a color, while a warning vector $*$ leaves the variable free.

We can rewrite the SP equations in terms of the distribution of warnings $\hat{Q}_{cz\to iu}(a)$, $a\in\{1,\dots,Q,*\}$. Since constraints have degree 2 we can view the messages $\hat{Q}_{cz\to iu}(a)$ as carried by the edge $\langle jv, iu\rangle$, where jv is the unique node in $\partial(cz)\setminus iu$. We thus make the replacement $\hat{Q}_{cz\to iu}(a)\to\hat{Q}_{jv\to iu}(a)$ and write down the SP equations on the induced graph of variable nodes. Moreover following [43] we seek solutions that do not depend on colors, and set $\hat{Q}_{jv\to iu}(a)\equiv\hat{Q}_{jv\to iu}$ for $a\in\{1,\dots,Q\}$. A calculation then shows that (148), (149) reduce to

$$\hat{Q}_{jv\to iu} = \frac{\sum_{l=1}^{Q}(-1)^l\binom{Q-1}{l}\prod_{kw\in\partial(jv)\setminus iu}(1-(l+1)\hat{Q}_{kw\to jv})}{\sum_{l=0}^{Q-1}(-1)^l\binom{Q}{l+1}\prod_{kw\in\partial(jv)\setminus iu}(1-(l+1)\hat{Q}_{kw\to jv})}, \tag{57}$$

and

$$\hat{Q}_{jv\to iu}(*) = 1 - Q\,\hat{Q}_{jv\to iu}. \tag{58}$$

Now, recall that the degrees of nodes of the induced graph are Poisson(2α) integers. *From now on we set* $c\equiv 2\alpha$. We solve (57), (58) under the assumption that the messages emanating from node jv are i.i.d. copies of a random variable $\hat{Q}_v$ with a distribution that depends only on the position v. Fix a position z, pick an integer d according to a Poisson(c), and pick integers $k_1,\dots,k_d$ i.i.d. uniform in $\{-w+1,\dots,w-1\}$. We have[7]

$$\hat{Q}_z = \frac{\sum_{l=1}^{Q}(-1)^l\binom{Q-1}{l}\prod_{1=1}^{d}(1-(l+1)\hat{Q}^{(i)}_{z+k_i})}{\sum_{l=0}^{Q-1}(-1)^l\binom{Q}{l+1}\prod_{i=1}^{d}(1-(l+1)\hat{Q}^{(i)}_{z+k_i})}, \tag{59}$$

and

$$\hat{Q}_z(*) = 1 - Q\,\hat{Q}_z. \tag{60}$$

Here, the relevant boundary conditions are taken into account by setting $\hat{Q}_z = 0$ for $z\le -\frac{L}{2}$ and $z>\frac{L}{2}$. These equations are solved numerically by population dynamics. This then allows to compute the ensemble average of the complexity,

$$\Sigma_{L,w}(c) = \frac{1}{L}\sum_{z=-\frac{L}{2}+1}^{\frac{L}{2}}\left(\mathbb{E}\big[\Sigma_z^{\mathrm{var}}\big] - \frac{c}{2}\mathbb{E}\big[\Sigma_z^{\mathrm{edge}}\big]\right), \tag{61}$$

[7] Interpreted as equalities between random variables.

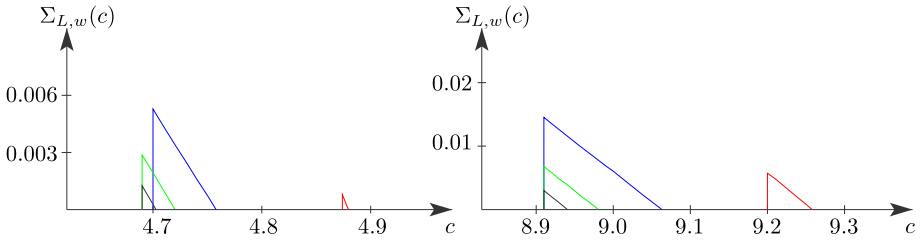

Fig. 7 Average complexity for the $[1000, Q, c, 3, L]$ ensembles with $Q = 3$ (*left*) and $Q = 4$ (*right*). Here $L = 10, 20, 40, 80$ from right to left. See corresponding Table 3 for numerical values of thresholds

Table 3 Thresholds computed by population dynamics for the individual and coupled ensembles for ensembles $[1000, Q, c, 3, L]$

Q	3	3	4	4
Individual	c_{SP}	c_s	c_{SP}	c_s
$L = 1$	4.42	4.69	8.27	8.90
Coupled	$c_{\mathrm{SP},L,3}$	$c_{s,L,3}$	$c_{\mathrm{SP},L,3}$	$c_{s,L,3}$
$L = 10$	4.874	4.879	9.20	9.25
$L = 20$	4.70	4.75	8.91	9.06
$L = 40$	4.69	4.72	8.91	8.98
$L = 80$	4.69	4.70	8.91	8.93

with

$$\Sigma_z^{\mathrm{var}} = \ln\left\{\sum_{l=0}^{Q-1}(-1)^l\binom{Q}{l+1}\prod_{i=1}^{d}\bigl(1-(l+1)\hat{Q}_{z+k_i}^{(i)}\bigr)\right\}, \tag{62}$$

$$\Sigma_z^{\mathrm{edge}} = \ln\bigl\{1-Q\hat{Q}_z^{(1)}\hat{Q}_{z+k}^{(2)}\bigr\}. \tag{63}$$

The numerical results are similar to those for the coupled K-SAT model. Figure 7 shows that the complexity is positive in an interval $[c_{\mathrm{SP},L,w}, c_{s,L,w}]$ which signals the existence of exponentially many pure states. Beyond $c_{s,L,w}$ the complexity becomes negative which means that the graph instances are not colorable w.h.p. Table 3 gives the values of the thresholds $c_{\mathrm{SP},L,w}$ and $c_{s,L,w}$. Again, the observations suggest that $c_{s,L,w} \downarrow c_s$ as L increases, and that threshold saturation takes place, namely $c_{\mathrm{SP},L,w} \to c_s$ as $L \gg w \gg 1$. The same comments than in K-SAT apply and we do not repeat them here.

4.2 Survey Propagation for Large Q

4.2.1 Fixed Point Equations

The large Q analysis for the individual system [43] is extended to the coupled model. In this regime c_s is $O(Q \ln Q)$ therefore it is natural to set

$$c = \hat{c}\, Q \ln Q, \tag{64}$$

and to analyze (59) for $\hat{c}$ fixed. In this limit the node degrees concentrate on $d \approx Q \ln Q$ with a fluctuation $O(\sqrt{Q \ln Q})$. Therefore, we assume that in the expression

$$\prod_{i=1}^{d} \big(1 - (l+1)\hat{Q}_{z+k_i}^{(i)}\big) = e^{\sum_{i=1}^{d} \ln\{1-(l+1)\hat{Q}_{z+k_i}^{(i)}\}}, \tag{65}$$

we can replace the sum over a large number of terms by its average,

$$e^{\frac{\hat{c}Q\ln Q}{2w-1}\sum_{k=-w+1}^{w-1}\mathbb{E}[\ln\{1-(l+1)\hat{Q}_{z+k}\}]}. \tag{66}$$

In this expression the average over d and $k_1, \ldots, k_d$ has been carried out and the remaining expectation is over $\hat{Q}_z$. Since the product (65) enters in (59), we conclude that Q_z concentrates on its average. Thus, setting

$$\mathbb{E}[\hat{Q}_z] = \hat{q}_z \tag{67}$$

for the average warning probability, we find

$$\hat{q}_z = \frac{\sum_{l=1}^{Q}(-1)^l \binom{Q-1}{l} \exp(\frac{\hat{c}Q\ln Q}{2w-1}\sum_{k=-w+1}^{w-1}\ln\{1-(l+1)\hat{q}_{z+k}\})}{\sum_{l=0}^{Q-1}(-1)^l \binom{Q}{l+1} \exp(\frac{\hat{c}Q\ln Q}{2w-1}\sum_{k=-w+1}^{w-1}\ln\{1-(l+1)\hat{q}_{z+k}\})}. \tag{68}$$

It can be checked self-consistently from the solutions of the fixed point equation that $\hat{q}_z = O(Q^{-1})$ and therefore for $l = O(1)$ the log in (68) can be linearized, while the terms with higher l are damped. Linearizing the log the sum over l can be performed, and working with rescaled variables

$$\theta_z \equiv (\hat{c}Q\ln Q)\hat{q}_z, \tag{69}$$

we find

$$\theta_z = \hat{c}Q\ln Q \frac{\sum_{l=1}^{Q}(-1)^l \binom{Q-1}{l} \exp(-\frac{l+1}{2w-1}\sum_{k=-w+1}^{w-1}\theta_{z+k})}{\sum_{l=0}^{Q-1}(-1)^l \binom{Q}{l+1} \exp(-\frac{l+1}{2w-1}\sum_{k=-w+1}^{w-1}\theta_{z+k})}. \tag{70}$$

Let

$$F_Q(\theta) = Q\ln Q\, e^{-\theta}\frac{(1-e^{-\theta})^{q-1}}{1-(1-e^{-\theta})^q}. \tag{71}$$

The fixed point equation takes the simple form

$$\theta_z = \hat{c}F_Q\left(\frac{1}{2w-1}\sum_{k=-w+1}^{w-1}\theta_{z+k}\right). \tag{72}$$

These equations must be solved with the boundary condition $\theta_z = 0$ for $z \le -\frac{L}{2}$ and $z > \frac{L}{2}$ in order to find the average warning probability profiles.

4.2.2 Average Complexity

Proceeding as above we find from (62), (63)

$$\mathbb{E}\big[\Sigma_z^{\text{var}}\big] = \ln\left\{\sum_{l=0}^{q-1}(-1)^l\binom{Q}{l+1}e^{\frac{\hat{c}Q\ln Q}{2w-1}\sum_{k=-w+1}^{w-1}\ln\{1-(l+1)\hat{q}_{z+k}\}}\right\}, \tag{73}$$

$$\mathbb{E}\big[\Sigma_z^{\text{cons}}\big] = \frac{1}{2w-1}\sum_{k=-w+1}^{w-1}\ln\{1-Q\hat{q}_z\hat{q}_{z+k}\}. \tag{74}$$

As before since $\hat{q}_z = O(Q^{-1})$ we can linearize the log in the exponential of the first equation and the one in the second equation. Then working with the rescaled variables (41), straightforward algebra leads to an average complexity (61) given by

$$\Sigma_{L,w}(c) = \frac{1}{L} \sum_{z=-\frac{L}{2}+1}^{\frac{L}{2}} \left[\ln\left\{1 - \left(1 - e^{-\frac{1}{2w-1}\sum_{k=-w+1}^{w-1}\theta_{z+k}}\right)^{Q}\right\} + \frac{\theta_z}{2\hat{c}\ln Q}\frac{1}{2w-1}\sum_{k=-w+1}^{w-1}\theta_{z+k}\right]. \tag{75}$$

This functional is defined for profiles that satisfy the boundary condition $\theta_z = 0$ for $z \le -\frac{L}{2}$ and $z > \frac{L}{2}$. The consistency of our approximations can be checked by noticing that the stationary points of (75) are precisely given by the solutions of the fixed point equation (72).

4.3 Solutions for Large Q

The discussion is quite similar to the case of K-SAT so we will be brief. By setting $L = w = 1$, we recover the fixed point equation of the individual system which is $\theta = \hat{c} F_Q(\theta)$. Fixed points are stationary points of the complexity as a function of θ,

$$\Sigma_{1,1}(\hat{c}, \theta) = \ln\left\{1 - \left(1 - e^{-\theta}\right)^{Q}\right\} + \frac{\theta^2}{2\hat{c}\ln Q}. \tag{76}$$

This function controls the existence and nature of the fixed points. At $\theta = 0$ it has a minimum for all $\hat{c}$ which corresponds to a trivial stable fixed point and a vanishing complexity $\Sigma_{1,1}(\hat{c}) = 0$. It is unique for $\hat{c} < \hat{c}_{\rm SP} \doteq 1$. For $\hat{c} > \hat{c}_{\rm SP}$ a second minimum appears. This corresponds to a stable fixed point solution which form the branch $\theta_{\rm mst} \approx \hat{c}\ln Q + \ln(Q\ln Q)$. Replacing in (76) we find $\Sigma_{1,1}(\hat{c}) \approx (1 - \frac{\hat{c}}{2})\ln Q$. This is positive in the interval $\hat{c} \in [1, 2]$, and looses its meaning beyond $\hat{c}_s \doteq 2$ which is the static phase transition threshold.

Let us now turn to the coupled model. The same heuristic arguments than for K-SAT hold. In the regime $L \gg w \gg 1$ and with asymmetric boundary conditions $\theta_z \to 0$ for $z \to -\infty$ and $\theta \to \theta_{\rm mst}$ for $z \to +\infty$ we take a kink-like ansatz for the solutions of (72). Their total average complexity is given by a convex combination of, $\Sigma_{1,1}(\hat{c}, \theta = 0) = 0$ and $\Sigma_{1,1}(\hat{c}, \theta_{\rm mst}) = (1 - \frac{\hat{c}}{2})\ln Q$, with weights determined by the location of the kink center ξL. We have $\bar{\theta} \equiv \frac{1}{L}\sum_{z=-\frac{L}{2}+1}^{\frac{L}{2}} \theta_z = (\frac{1}{2} - \xi)\theta_{\rm mst}$ and $\Sigma_{\rm kink} \approx \frac{\bar{\theta}}{\theta_{\rm mst}}(1 - \frac{\hat{c}}{2})\ln Q$. The stable kink fixed point profile corresponds to $\bar{\theta} = 0$ and $\{\theta_z = 0\}$ for all $\hat{c} < 2$ which means that the complexity vanishes for $\hat{c} < 2$. Thus within this approximation the SP threshold saturates to the static phase transition threshold.

We solve (72) numerically with symmetric boundary conditions which enforce the profile to vanish at the end points of the chain. There exists a family of solution profiles $(\hat{c}(\bar{\theta}), \{\theta_z(\bar{\theta})\})$ parametrized by the total average warning probability $\bar{\theta} \equiv \frac{1}{L}\sum_{z=-\frac{L}{2}+1}^{\frac{L}{2}} \theta_z$. Figure 8 illustrates a sequence of van der Waals curves $\hat{c}(\bar{\theta})$ and Table 4 gives numerical values of their minima which determines $\hat{c}_{{\rm SP},L,w}$.

Finally, Fig. 9 displays warning and complexity profiles for $\hat{c}$ in the wiggles region. The results are analogous to those of K-SAT.

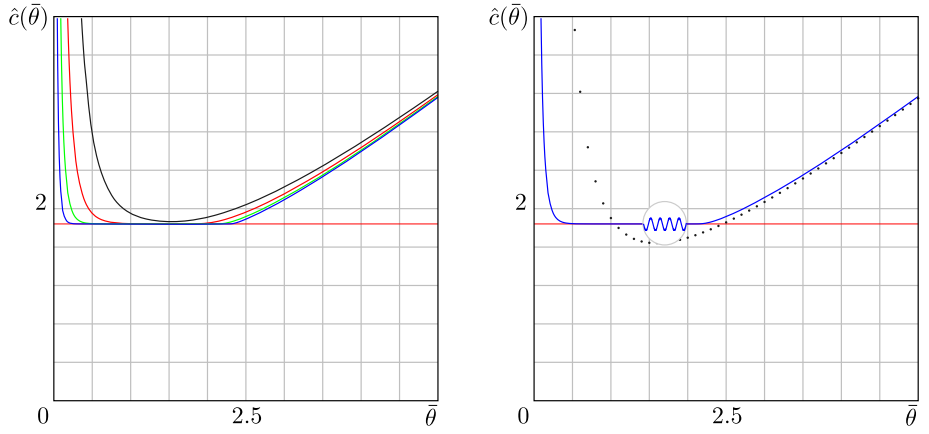

Fig. 8 *Left*: sequence of van der Waals curves for $K = 5$, $w = 3$ and $L = 10, 20, 40, 80$ (*top* to *bottom*). They converge to the individual system curve for $\theta \in [\theta_{\text{mst}}, +\infty]$. *Right*: a magnification of the plateau region for $L = 40$ shows the fine structure. The *dotted curve* is the individual system curve and the *horizontal line* corresponds to the phase transition threshold $\hat{\alpha}_s = 1.840980$

Table 4 SP thresholds of the individual ($L = w = 1$) and coupled ensembles ($L = 80$, $w = 2, 3, 4$) are found from the van der Waals curves. Threshold values $\hat{c}_s$ are from population dynamics. For $Q = 10$ we clearly see that the SP threshold saturates to $\hat{c}_s$ from below as w increases

Q	5	7	10
$\hat{c}_s$	1.840980	1.911260	1.635790
$\hat{c}_{\text{SP}}$	1.6411666	1.651565	1.949869
$\hat{c}_{\text{SP},80,2}$	1.839709	1.906734	1.939527
$\hat{c}_{\text{SP},80,3}$	1.840978	1.911213	1.949606
$\hat{c}_{\text{SP},80,4}$	1.840980	1.911260	1.949865

5 Proofs of Theorems 1 and 2

In this section we sketch the proofs of Theorems 1 and 2. The proof of Theorem 1 is straightforward and does not depend on the details of the model at hand. On the other hand that of Theorem 2 has to adapted for each model at hand.

5.1 Proof of Theorem 1

Recall that for the Hamiltonian of the open chain $\mathcal{H}_{\text{cou}}(\underline{x})$ in (3), $\underline{x} = (x_{iz})$ with $(i, z) \in \bigcup_{z=-\frac{L}{2}+1,\ldots,\frac{L}{2}+w-1} V_z$. It will be convenient to set $\underline{x} = (\underline{x}', \underline{x}'')$ where $\underline{x}' = (x_{iz}; z = -\frac{L}{2} + 1, \ldots, \frac{L}{2})$ and $\underline{x}'' = (x_{iz}; z = -\frac{L}{2} + 1, \ldots, \frac{L}{2} + w - 1)$. Recall also that the Hamiltonian $\mathcal{H}^{\text{per}}_{\text{cou}}(\underline{x}')$ of the periodic chain is given by the same expression (3) with $\underline{x}' = (x_{iz}; z = \frac{L}{2} + 1, \ldots, \frac{L}{2})$. Therefore the difference between the two Hamiltonians only comes because of the terms $\psi_{cz}(\underline{x}_{\partial cz})$ with $z = \frac{L}{2} - w + 2, \ldots, \frac{L}{2}$. In other words,

$$\left|\mathcal{H}_{\text{cou}}(\underline{x}', \underline{x}'') - \mathcal{H}^{\text{per}}_{\text{cou}}(\underline{x}')\right| \leq Mw, \tag{77}$$

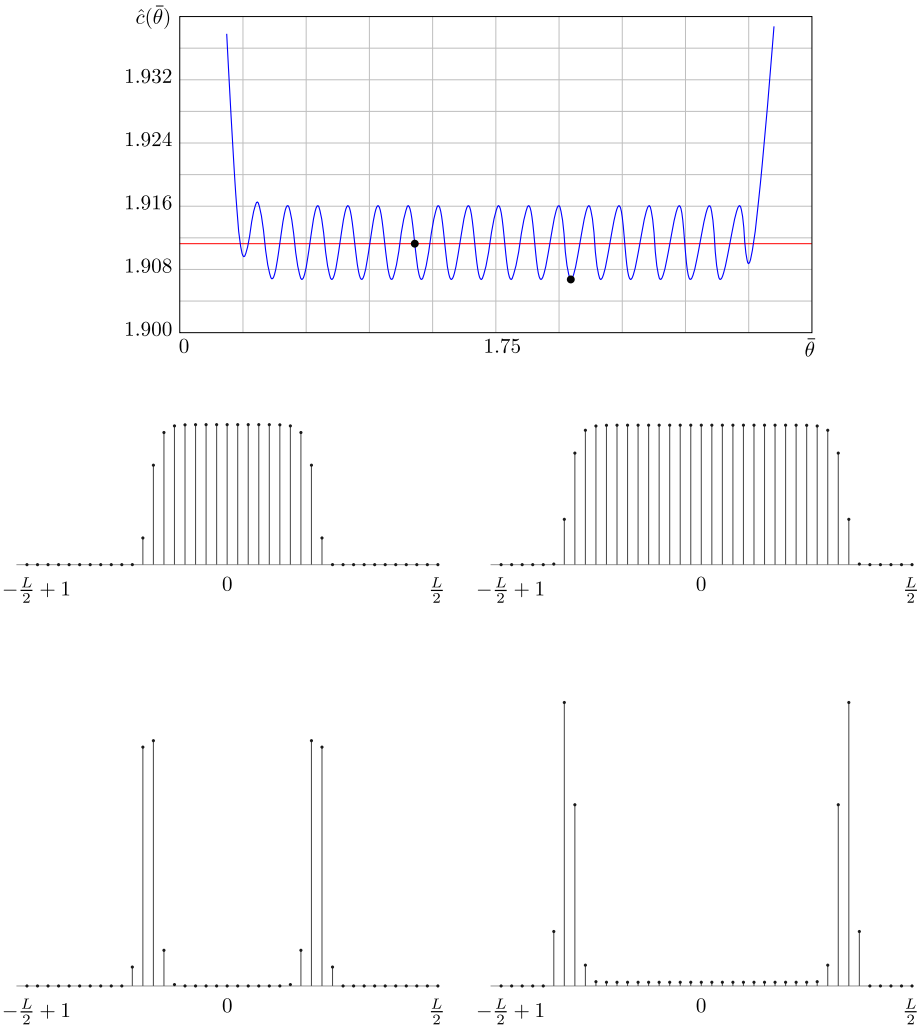

Fig. 9 van der Waals curves of the coupled system (*top*) for $Q = 7$, $w = 2$ and $L = 40$. *Middle* and *bottom left* are the warning and complexity profiles corresponding to the point with coordinates $(\bar{\theta}_l, \hat{c}_l) = (1.30125, 1.91260)$. Notice that $\hat{c}_l$ is near the phase transition threshold so that the complexity nearly vanishes except at the transition regions of the kink. The total average complexity nearly vanishes. *Middle* and *bottom right* are the warning and complexity density profiles corresponding to the point $(\bar{\theta}_r, \hat{c}_r) = (2.165, 1.906734)$. For the complexity profile at the *bottom right*, we see that in the *middle region* of the profile the height of the complexity density is $(1 - \frac{\hat{c}_r}{2}) \approx 0.047$ and the total average complexity is approximately given by $\frac{\bar{\theta}_r}{\theta_{\text{mst}}}(1 - \frac{\hat{c}_r}{2}) \ln Q$

for all $\underline{x}''$. As a result, we obtain

$$\mathcal{H}^{\text{per}}_{\text{cou}}\big(\underline{x}'\big) - Mw \leq \mathcal{H}_{\text{cou}}\big(\underline{x}', \underline{x}''\big) \tag{78}$$

and by taking the min, dividing by NL and taking the expectation, we deduce

$$e^{\text{per}}_{N,L,w}(\alpha) - \frac{\alpha w}{L} \leq e_{N,L,w}(\alpha). \tag{79}$$

To obtain the right-hand side inequality of (9), we recall that the periodic chain is obtained from the open chain by identifying the variable nodes at the right boundary with their corresponding ones at the left boundary. Now, since the open chain has more degrees of freedom and the set of check nodes of the open and periodic chain are identical, the minimum energy of the open chain is less than the one of the periodic chain. Let us make this observation more precise. We set $\underline{x}'_0 = (x_{iz}; z = -\frac{L}{2}+1, \dots, -\frac{L}{2}+w)$. Then,

$$\mathcal{H}_{\text{cou}}\big(\underline{x}', \underline{x}''\big)\big|_{\underline{x}''=\underline{x}'_0} = \mathcal{H}^{\text{per}}_{\text{cou}}\big(\underline{x}'\big). \tag{80}$$

Hence,

$$\min_{(\underline{x}', \underline{x}'')} \mathcal{H}_{\text{cou}}\big(\underline{x}', \underline{x}''\big) \le \min_{\underline{x}'} \mathcal{H}_{\text{cou}}\big(\underline{x}', \underline{x}''\big)\big|_{\underline{x}''=\underline{x}'_0} = \min_{\underline{x}'} \mathcal{H}^{\text{per}}_{\text{cou}}\big(\underline{x}'\big). \tag{81}$$

Taking the expectation and dividing by NL we get

$$e_{N,L,w}(\alpha) \le e^{\text{per}}_{N,L,w}(\alpha). \tag{82}$$

5.2 Proof of Theorem 2

As explained in Sect. 2 the proof that the limit exists, is continuous and non-decreasing, for the individual models is provided in [19] and is essentially the same for the coupled periodic chain. Here we prove the equality of the two limits (10). The following notation is convenient. For a given graph instance G (from some ensemble) we call $\mathcal{H}_G(\underline{x})$ the corresponding Hamiltonian. It always consists, as in (3), of a sum of terms $1 - \psi_{cz}(x_{\partial cz})$ over constraints $(c, z) \in G$. The ground state energy is equal to $\min_{\underline{x}} \mathcal{H}_G(\underline{x})$. To set up suitable interpolation procedures, it is convenient to first define three extra ensembles.

The "Connected" Ensemble This is essentially the individual $[N, K, \alpha]$ ensemble scaled by L. We have a set of LN variable nodes and a set of LM constraint nodes. Each constraint node has K edges connected u.a.r. to variable nodes. Expectations with respect to this ensemble are denoted by $\mathbb{E}_{\text{conn}}$. Because of the existence of the limit we have

$$\lim_{N\to+\infty} \frac{1}{LN} \mathbb{E}_{\text{conn}}\Big[\min_{\underline{x}} \mathcal{H}_G(\underline{x})\Big] = \lim_{N\to+\infty} e_N(\alpha), \tag{83}$$

for any fixed L.

The "Disconnected" Ensemble This is a variant of the individual $[N, K, \alpha]$ ensemble replicated L times. We place at positions $z = -\frac{L}{2}+1, \dots, \frac{L}{2}$, L disjoint sets of variable nodes V_z containing each N nodes. Each node from the set of LM constraint nodes is affected u.a.r. to a position $z = -\frac{L}{2}+1, \dots, \frac{L}{2}$. Note that the set $\tilde{C}_z$ of constraint nodes at position z has cardinality $M_z \sim \text{Bi}(LM, \frac{1}{L})$. Each node from $\tilde{C}_z$ has K edges that are connected u.a.r. to nodes in V_z. Expectations are denoted by $\mathbb{E}_{\text{disc}}$. Since each M_z is concentrated on M with a fluctuation $O(\sqrt{M})$, we can show by an argument similar to the proof of Theorem 1 that

$$\frac{1}{LN} \mathbb{E}_{\text{disc}}\Big[\min_{\underline{x}} \mathcal{H}_G(\underline{x})\Big] = e_N(\alpha) + O\big(N^{-1/2}\big), \tag{84}$$

where $O(N^{-1/2})$ is uniform in L.

The "Ring" Ensemble This is a variant of the periodic chain in Sect. 2. We place at positions $z = -\frac{L}{2}+1, \dots, \frac{L}{2}$, L disjoint sets of variable nodes V_z, each containing N nodes. Now we have a set of LM constraint nodes. Each constraint node is affected to a position $z = -\frac{L}{2}+1, \dots, \frac{L}{2}$ u.a.r. and (say the position is z) its K edges are connected u.a.r. to the set of variables $\bigcup_{k=0}^{w-1} V_{z+k \bmod L}$. Note that the sets $\tilde{C}_z$ of constraint nodes have cardinalities $M_z \sim \mathrm{Bi}(LM, \frac{1}{L})$. We denote by $\mathbb{E}_{\mathrm{ring}}$ the expectation with respect to this ensemble. Since each M_z is concentrated on M with a fluctuation $O(\sqrt{M})$, an argument similar to the proof of Theorem 1 shows that

$$\frac{1}{LN}\mathbb{E}_{\mathrm{ring}}\Big[\min_{\underline{x}} \mathcal{H}_G(\underline{x})\Big] = e^{\mathrm{per}}_{N,L,w}(\alpha) + O\big(N^{-1/2}\big), \tag{85}$$

where $O(N^{-1/2})$ is uniform in L (and depends on w).

We will show

$$\mathbb{E}_{\mathrm{conn}}\Big[\min_{\underline{x}} \mathcal{H}_G(\underline{x})\Big] \le \mathbb{E}_{\mathrm{ring}}\Big[\min_{\underline{x}} \mathcal{H}_G(\underline{x})\Big] \le \mathbb{E}_{\mathrm{disc}}\Big[\min_{\underline{x}} \mathcal{H}_G(\underline{x})\Big], \tag{86}$$

which allows to conclude the proof of the theorem by using (83), (84), (85).

Left Inequality in (86) We build a sequence of interpolating "r-ensembles", $r = 0, \dots, LM$, interpolating between the ring ($r = 0$) and connected ($r = LM$) ensembles. We have two sets of LM constraint and LN variable nodes. The variable nodes are organized into L disjoint sets V_z each containing N nodes, placed along the positions $z = -\frac{L}{2}+1, \dots, \frac{L}{2}$. Expectation with respect to the r-ensemble is denoted by $\mathbb{E}_r$. To sample a graph G_r from this ensemble we first take r nodes—called type 1—from the set of LM constraint nodes. Each one has K edges which are connected u.a.r. to the set of LN variable nodes. For the remaining $LM - r$ constraint nodes—called type 2—we proceed as follows: each one is affected u.a.r. to a position z, and its K edges are then connected u.a.r. to the wN variable nodes in $\bigcup_{k=0}^{w-1} V_{z+k \bmod L}$. We claim that for $1 \le r \le LM$,

$$\mathbb{E}_r\Big[\min_{\underline{x}} \mathcal{H}_{G_r}(\underline{x})\Big] \le \mathbb{E}_{r-1}\Big[\min_{\underline{x}} \mathcal{H}_{G_{r-1}}(\underline{x})\Big]. \tag{87}$$

Clearly this implies the left inequality in (86). Let us prove this claim. Take a random graph G_r and delete u.a.r. a constraint from the type 1 nodes: this yields an intermediate graph $\tilde{G}$. One can go back to a random graph G_r by adding back a type 1 node according to the above rules, or one can go to a random graph G_{r-1} by adding back a type 2 node according to the above rules. We will prove that conditioned on any realization of $\tilde{G}$ we have

$$\mathbb{E}_r\Big[\min_{\underline{x}} \mathcal{H}_{G_r}(\underline{x}) \,\Big|\, \tilde{G}\Big] \le \mathbb{E}_{r-1}\Big[\min_{\underline{x}} \mathcal{H}_{G_{r-1}}(\underline{x}) \,\Big|\, \tilde{G}\Big]. \tag{88}$$

Claim (87) follows by averaging over $\tilde{G}$. We now prove (88) for K-SAT and Q-coloring separately.

K-SAT Consider the set of "optimal assignments" $\underline{x}$ that minimize $\mathcal{H}_{\tilde{G}}(\underline{x})$. We say that a variable is *frozen* iff it takes the same value for all optimal assignments. We call $\mathcal{F}$ the set of variable nodes with frozen variables and $\mathcal{F}_z = \mathcal{F} \cap V_z$. Now consider adding a new constraint node n to the graph $\tilde{G}$. This will cost an extra energy iff the node n connects only to frozen variable nodes *and* does not satisfy them. For such an event we have

$$\min_{\underline{x}} \mathcal{H}_{\tilde{G}\cup n}(\underline{x}) - \min_{\underline{x}} \mathcal{H}_{\tilde{G}}(\underline{x}) = 1. \tag{89}$$

When the node n is connected u.a.r. to the LN variable nodes (n is type 1) this event has probability $\frac{1}{2^K}(\frac{|\mathcal{F}|}{LN})^K$. Thus

$$\mathbb{E}_r\Big[\min_{\underline{x}} \mathcal{H}_{G_r}(\underline{x}) \mid \tilde{G}\Big] - \min_{\underline{x}} \mathcal{H}_{\tilde{G}}(\underline{x}) = \frac{1}{2^K}\left(\frac{|\mathcal{F}|}{LN}\right)^K. \tag{90}$$

Similarly when the node n is affected u.a.r. to a position z and then connected u.a.r. to $\bigcup_{k=0}^{w-1} V_{z+k \bmod L}$ (n is type 2) we get

$$\mathbb{E}_{r-1}\Big[\min_{\underline{x}} \mathcal{H}_{G_{r-1}}(\underline{x}) \mid \tilde{G}\Big] - \min_{\underline{x}} \mathcal{H}_{\tilde{G}}(\underline{x}) = \frac{1}{L}\sum_{z=-\frac{L}{2}+1}^{\frac{L}{2}} \frac{1}{2^K}\left(\frac{1}{wN}\sum_{k=0}^{w-1}|\mathcal{F}_{z+k \bmod L}|\right)^K. \tag{91}$$

Claim (88) follows from the last two equations, convexity of x^K for $x \geq 0$, and

$$|\mathcal{F}| = \sum_{z=-\frac{L}{2}+1}^{\frac{L}{2}} \frac{1}{w}\sum_{k=0}^{w-1}|\mathcal{F}_{z+k \bmod L}|. \tag{92}$$

Q-Coloring The proof is similar. Consider the set of "optimal colorings" that minimize $\mathcal{H}_{\tilde{G}}(\underline{x})$. We define an equivalence relation between variable nodes: we say that two nodes are equivalent iff their two colors are identical for all optimal assignments. Let $\mathcal{F}^j$, $1 \leq j \leq J$, be the equivalence classes of nodes and let $\mathcal{F}_z^j = \mathcal{F}^j \cap \mathcal{V}_z$. Now, assume we add a random constraint node n to $\tilde{G}$. We have $\min_{\underline{x}} \mathcal{H}_{\tilde{G}\cup n}(\underline{x}) - \min_{\underline{x}} \mathcal{H}_{\tilde{G}}(\underline{x}) = 1$ only when n chooses its two variables from the same equivalence class; otherwise the energy difference is zero. Thus we obtain

$$\mathbb{E}_r\Big[\min_{\underline{x}} \mathcal{H}_{G_r}(\underline{x}) \mid \tilde{G}\Big] - \min_{\underline{x}} \mathcal{H}_{\tilde{G}}(\underline{x}) = \sum_{i=1}^{J}\left(\frac{|\mathcal{F}^j|}{LN}\right)^2, \tag{93}$$

and

$$\mathbb{E}_{r-1}\Big[\min_{\underline{x}} \mathcal{H}_{G_{r-1}}(\underline{x}) \mid \tilde{G}\Big] - \min_{\underline{x}} \mathcal{H}_{\tilde{G}}(\underline{x}) = \frac{1}{L}\sum_{z=-\frac{L}{2}}^{\frac{L}{2}}\sum_{j=1}^{J}\left(\frac{1}{wN}\sum_{k=0}^{w-1}|\mathcal{F}_{z+k \bmod L}^j|\right)^2. \tag{94}$$

Claim (88) then follows from the last two equations and convexity of x^2.

Right Inequality in (86) We construct new r-ensembles, $r = 0, \ldots, LM$ that now interpolate between the disconnected ($r = 0$) and the ring ($r = LM$) ensembles. A random graph G_r is constructed as follows. We have a set of LM constraint nodes and a set of LN variable nodes organized into L disjoint sets V_z each containing N nodes, placed along positions z. We first take r constraint nodes, called type 1. Each of them is affected u.a.r. to a position z, and its K edges are connected u.a.r. to variable nodes in V_z. Next, the remaining $LM - r$ constraints nodes—called type 2—are each affected u.a.r. to a position z and its K edges are connected u.a.r. to wN nodes in $\bigcup_{k=0}^{w-1} V_{z+k \bmod L}$. Note that at each position there are $\mathrm{Bi}(r, \frac{1}{L})$ type 1 nodes and $\mathrm{Bi}(LM - r, \frac{1}{L})$ type 2 nodes, so in total there are $\mathrm{Bi}(LM, \frac{1}{L})$ constraint nodes. Similarly to the previous interpolation we will prove

$$\mathbb{E}_r\Big[\min_{\underline{x}} \mathcal{H}_{G_r}(\underline{x})\Big] \leq \mathbb{E}_{r-1}\Big[\min_{\underline{x}} \mathcal{H}_{G_{r-1}}(\underline{x})\Big]. \tag{95}$$

This inequality implies the upper bound in (86). To prove (95), as before, we consider the random graph $\tilde{G}$ obtained by deleting u.a.r. a type 1 node from G_r. From $\tilde{G}$ one gets a

random graph G_r by adding back a type 1 node, or one gets a graph G_{r-1} by adding back a type 2 node instead. We first prove that

$$\mathbb{E}_r\Big[\min_{\underline{x}} \mathcal{H}_{G_r}(\underline{x}) \mid \tilde{G}\Big] \le \mathbb{E}_{r-1}\Big[\min_{\underline{x}} \mathcal{H}_{G_{r-1}}(\underline{x}) \mid \tilde{G}\Big], \tag{96}$$

and then by averaging over graphs $\tilde{G}$ we get (95). Let us briefly sketch the derivation of (96).

K-SAT We use the same sets $\mathcal{F}_z$ of frozen variables at position z corresponding to the ground state configurations of $\mathcal{H}_{\tilde{G}}(\underline{x})$. We have

$$\mathbb{E}_r\Big[\min_{\underline{x}} \mathcal{H}_{G_r}(\underline{x}) \mid \tilde{G}\Big] - \min_{\underline{x}} \mathcal{H}_{\tilde{G}}(\underline{x}) = \frac{1}{L} \sum_{z=-\frac{L}{2}+1}^{\frac{L}{2}} \frac{1}{2^K} \left(\frac{|\mathcal{F}_z|}{N}\right)^K, \tag{97}$$

and

$$\mathbb{E}_{r-1}\Big[\min_{\underline{x}} \mathcal{H}_{G_{r-1}}(\underline{x}) \mid \tilde{G}\Big] - \min_{\underline{x}} \mathcal{H}_{\tilde{G}}(\underline{x}) = \frac{1}{L} \sum_{z=-\frac{L}{2}+1}^{\frac{L}{2}} \frac{1}{2^K} \left(\frac{1}{wN} \sum_{k=0}^{w-1} |\mathcal{F}_{z+k \bmod L}|\right)^K. \tag{98}$$

Estimate (96) then follows by the convexity of the function x^K for $x \ge 0$.

Q-Coloring We use the same equivalence relation between variable nodes and sets $\mathcal{F}_z^j$. We have

$$\mathbb{E}_r\Big[\min_{\underline{x}} \mathcal{H}_{G_r}(\underline{x}) \mid \tilde{G}\Big] - \min_{\underline{x}} \mathcal{H}_{\tilde{G}}(\underline{x}) = \frac{1}{L} \sum_{z=-\frac{L}{2}+1}^{\frac{L}{2}} \sum_{i=1}^{J} \left(\frac{|\mathcal{F}_z^j|}{N}\right)^2, \tag{99}$$

and

$$\mathbb{E}_{r-1}\Big[\min_{\underline{x}} \mathcal{H}_{G_{r-1}}(\underline{x}) \mid \tilde{G}\Big] - \min_{\underline{x}} \mathcal{H}_{\tilde{G}}(\underline{x}) = \frac{1}{L} \sum_{z=-\frac{L}{2}+1}^{\frac{L}{2}} \sum_{j=1}^{J} \left(\frac{1}{wN} \sum_{k=0}^{w-1} |\mathcal{F}_{z+k \bmod L}^j|\right)^2. \tag{100}$$

Again, estimate (96) then follows from the convexity of x^2.

6 Dynamical and Condensation Thresholds

The SP formalism says nothing about the relative sizes (internal entropy) of clusters of solutions and consequently does not take into account which of them are "relevant" to the uniform measure over zero energy solutions. For similar reasons, it is not clear that the SP threshold has particular algorithmic significance. These issues are partly addressed by the more elaborate entropic cavity method [20–22]. It predicts the existence of the dynamical and condensation thresholds α_d and α_c. The dynamical threshold is believed to separate a phase ($\alpha < \alpha_d$) where the uniform measure is essentially supported on one well connected cluster of dominant entropy, and a phase ($\alpha_d < \alpha < \alpha_c$) where the measure is supported on an exponential number of clusters with equal internal entropy. For $\alpha > \alpha_c$ the measure condenses on a "handful" of clusters of dominant entropy. The condensation threshold is a static thermodynamic transition in the sense that the total ground state entropy has a non-analyticity as a function of α. These thresholds were first computed for CSP in [23], where

Table 5 Thresholds of individual and coupled K-SAT model for $L = 80$ and $w = 3$. The condensation and SAT-UNSAT thresholds correspond to non analyticities of the entropy and ground state energy and remain unchanged (for $L \to +\infty$). Already for $w = 3$ the dynamical and SP thresholds saturate very close to α_c and α_s

K	α_{SP}	$\alpha_{\mathrm{SP},80,3}$	α_d	$\alpha_{d,80,3}$	α_c	$\alpha_{c,80,3}$	α_s	$\alpha_{s,80,3}$
3	3.927	4.268	3.86	3.86	3.86	3.86	4.267	4.268
4	8.30	9.94	9.38	9.55	9.55	9.56	9.93	10.06

their algorithmic significance is also discussed. See also [24, 25] for recent related algorithmic results.

We have computed the dynamical and condensation thresholds of coupled CSP. Let us denote them $\alpha_{d,L,w}$ and $\alpha_{c,L,w}$ (with w fixed). We observe that as L increases $\alpha_{c,L,w} \to \alpha_c$. This observation is consistent with the following rigorous result that we prove in Appendix A: the thermodynamic limit of the free energy (at finite temperature) of the chain is identical to that of the individual model. From the free energy one can formally obtain the entropy by differentiating the free energy with respect to temperature. The result about the free energy then suggests that the zero temperature entropy of the chain and individual models have the same non-analyticity points as a function of the constraint density. The second important observation is that in the regime $1 \ll w \ll L$ we find $\alpha_{d,L,w} \to \alpha_c$. Thus the dynamical threshold saturates towards the condensation threshold.[8]

The dynamical and condensation thresholds are analogous to the dynamical and condensation temperatures of p-spin glass models for $p \geq 3$, and to the glassy and Kauzmann transition temperatures in structural glasses [26–28]. One expects that a similar saturation of the dynamical towards the condensation temperature holds for coupled p-spin glass models on complete graphs for $p \geq 3$. On the other hand, for $p = 2$ the replica symmetry breaking transition is continuous, there is no dynamical temperature, and spatial coupling is not expected to modify the phase diagram.

Table 5 summarizes all the behaviors of the SP, SAT-UNSAT, dynamical and condensation thresholds for the K-SAT problem. The situation for coloring is similar.

7 An Application of Threshold Saturation to Algorithmic Lower Bounds

We briefly discuss a methodology, that uses coupled CSP ensembles, for proving lower bounds on the static phase transition threshold of individual CSP ensembles. We illustrate it with simple examples and show how threshold saturation can help. These examples do not reach the best known lower bounds, but they serve well to illustrate a new methodology for attacking the problem. We keep the discussion at an informal level.

Given a CSP from an individual ensemble, one usually tries to devise an algorithm that provably finds solutions w.h.p. for $\alpha < \alpha_{\mathrm{alg}}$. This then implies $\alpha_{\mathrm{alg}} < \alpha_s$. Consider now the coupled ensemble, and apply the same algorithm. Call $\alpha_{\mathrm{alg},L,w}$ the algorithmic threshold for the existence w.h.p. of solutions and set $\alpha_{\mathrm{alg},w} = \lim_{L\to+\infty} \alpha_{\mathrm{alg},L,w}$. From Theorems 1 and 2 we know that the coupled ensemble has the same static phase transition threshold as the individual one, when $L \to +\infty$. Therefore one certainly has the lower bound $\alpha_{\mathrm{alg},w} < \alpha_s$. The point is that for well chosen algorithms an improvement of the bound may occur, namely

[8] Note that for $K = 3$ we already have $\alpha_d = \alpha_c$ for the individual ensemble.

Table 6 *First line*: phase transition threshold for K-XORSAT. *Second line*: leaf removal threshold for the uncoupled case. *Third line*: leaf removal threshold for a coupled chain with $w = 5$, $L = 80$

K	3	4	5	7
α_s	0.917	0.976	0.992	0.999
α_{lr}	0.818	0.772	0.701	0.595
$\alpha_{lr,L=80,w=5}$	0.917	0.977	0.992	0.999

$\alpha_{\text{alg}} < \alpha_{\text{alg},w} < \alpha_s$, and one would expect to get the best lower bounds by increasing w. A well chosen algorithm is one that shows a "threshold improvement" or even saturation phenomenon. Somehow the "seed" provided by the reduced hardness near the boundaries should grow and propagate in the bulk.

Below we illustrate the idea with three simple peeling algorithms applied to K-XORSAT, K-SAT and Q-COL.

K-XORSAT This case provides the best illustration. The individual model has a static phase transition at α_s, and a clustering transition at α_{SP} with a complexity counting clusters in the interval $[\alpha_{\text{SP}}, \alpha_s]$. In Appendix A (Theorem 5) we show that the coupled and individual ensembles have the same phase transition threshold α_s for even K (for odd K the proof breaks down but the result is presumably true). Now consider the "leaf removal" algorithm. As long as there is a leaf variable node remove it, and remove the attached constraint node with its emanating edges. If this process ends with an empty graph the instance is satisfiable. It is known that this algorithm is equivalent to BP message passing, and the density evolution analysis leads to the fixed point equation

$$x = \big(1 - \exp(-\alpha K x)\big)^{K-1}. \tag{101}$$

Here, x is interpreted as the probability (when the number of iterations goes to infinity) that a constraint node is not removed. There is a threshold α_{lr} above which (101) has non-trivial fixed points (i.e., the fraction of remaining variables is positive), so we get a lower bound $\alpha_{\text{lr}} < \alpha_s$. For the coupled ensemble the density evolution analysis yields the one-dimensional fixed point equations

$$x_z = \left\{ \frac{1}{w} \sum_{l=0}^{w-1} \left(1 - \exp\left(-\frac{\alpha K}{w} \sum_{k=0}^{w-1} x_{z+k-l} \right) \right) \right\}^{K-1}, \tag{102}$$

with boundary condition $x_z = 0$ for z at the boundaries. Solving for the non-trivial kink solutions numerically, we indeed observe $\alpha_{\text{lr}} < \alpha_{\text{lr},w} < \alpha_s$. Table 6 shows the threshold improvement for $w = 5$ and the first few values of K. In fact the leaf removal threshold even saturates $\alpha_{\text{lr},w} \uparrow \alpha_s$ as $w \to +\infty$. This is not surprising since for XORSAT the SP formalism leads to the same fixed point equations (but with a different interpretation for x and x_z) [12, 34]. In particular there is a complexity $\Sigma_{\text{xorsat}}(\alpha) > 0$ for $\alpha \in [\alpha_{\text{SP}}, \alpha_s]$ counting the number of clusters of solutions in Hamming space with $\alpha_{\text{SP}} = \alpha_{\text{lr}}$ and $\Sigma_{\text{xorsat}}(\alpha_s) = 0$. Note that for large K one finds $\alpha_{\text{lr}} = \ln K/K + \ln\ln K/K + 1/K + o(1/K)$ and $\alpha_s = 1 + o(1)$.

K-SAT Let us now turn to K-SAT and consider the "pure literal rule" algorithm [32, 33]. Consider variable nodes that have only one type of edge—dashed or full—attached to them. As long as there are such nodes (called "pure") set the variable to the value which satisfies all the attached constraints and remove these constraints and their edges. Continue until no

"pure" node remains. If no constraint node remains then the algorithm succeeds in finding a satisfying assignment. This algorithm can be cast in a message passing form and can be analyzed by the density evolution method [40]. The net result is that the pure literal rule succeeds w.h.p. for $\alpha < \alpha_{\rm pl}$ such that

$$x = \left(1 - \exp\left(-\frac{\alpha K}{2} x\right)\right)^{K-1} \tag{103}$$

has a unique fixed point $x = 0$. We now take coupled instances from the ensemble defined in Sect. 2. In order to analyze the pure literal rule we can think of extending the chain to $\mathbb{Z}$ with "pure" variable nodes for $z \le -\frac{L}{2}$ and $\ge \frac{L}{2} + w$. The peeling of constraints attached to pure nodes will propagate inside the chain as long as α is not too large. The analysis yields the one-dimensional fixed point equations

$$x_z = \left\{\frac{1}{w}\sum_{l=0}^{w-1}\left(1 - \exp\left(-\frac{\alpha K}{2w}\sum_{k=0}^{w-1} x_{z+k-l}\right)\right)\right\}^{K-1} \tag{104}$$

with boundary condition $x_z = 0$ for z at the boundaries. Note that (103), (104) are the same as (101), (102) with the replacement $\alpha \to \alpha/2$. Therefore the pure literal thresholds $\alpha_{\rm pl}$, $\alpha_{{\rm pl},w}$ for the individual and coupled ensembles are obtained just by doubling the XORSAT thresholds. For example for $K = 3$ we have $\alpha_{\rm pl} \approx 1.636 < \alpha_{{\rm pl},w=5,L=80} \approx 1.835 < \alpha_s \approx 4.26$, a modest improvement. Interestingly when $K \to +\infty$ we have

$$\alpha_{\rm pl} \doteq \frac{2\ln K}{K} \quad \text{but } \alpha_{{\rm pl},w} \to 2 \text{ as } w \to +\infty. \tag{105}$$

Of course this is still a ridiculous lower bound since we know that $\alpha_s \doteq 2^K \ln 2$.

Q-COL Finally we discuss a similar peeling algorithm for Q-COL. This algorithm determines the Q-core of a graph G and has been analyzed by the method of differential equations [35]. Here we discuss the algorithm from the message passing point of view. Assume there exists a node i in G that has degree less than Q. Clearly, if we can color the graph $G \setminus i$ with Q colors, then G can also be colored with Q colors. Hence, finding a Q-coloring for G is equivalent to finding a Q-coloring for $G \setminus i$. As a result, we can peel the node i from G and continue this process until the final graph (the Q-core) has no more nodes of degree less than Q. If the final graph is empty then the algorithm succeeds otherwise it fails.

Now, consider the following message passing rule. At time $t \in \{1, 2, \ldots\}$, assign to each edge $\langle i, j\rangle \in E$ two messages $\mu^t_{i\to j}$ and $\mu^t_{j\to i}$. The messages at time $t+1$ are evolved from the ones at time t via the following procedure:

1. At time 0, initialize all the messages to 0.
2. At time $t+1$,

$$\mu^{t+1}_{i\to j} = \mathbb{1}\left(\sum_{h\in\partial i\setminus j} \mu^t_{h\to i} < Q - 1\right).$$

The above message passing rule is equivalent to the peeling algorithm in the sense that when $\mu^t_{i\to j} = 1$, the vertex i would have been peeled by the algorithm some time before t and if $\mu^t_{i\to j} = 0$, the vertex i would not have been peeled by the algorithm up to time t.

Define $x_t = \mathbb{P}(\mu^t_{i\to j} = 1)$. we derive the density evolution equation that relates x_{t+1} to x_t. Let G be randomly chosen from $G(N, \frac{c}{N})$ with N very large. Fix an edge $\langle i, j\rangle$. Observe that $\mu^{t+1}_{i\to j} = 1$ if and only if the number of incoming messages that have value 1 is $\le Q - 2$.

Table 7 *First line*: static phase transition threshold for Q-COL. *Second line*: peeling algorithm threshold for the uncoupled case. *Third line*: peeling algorithm threshold for a coupled chain with $w = 5$, $L = 80$

Q	3	4	5	7
c_s	4.69	8.90	13.69	24.46
c_{p}	3.35	5.14	6.79	9.87
$c_{p,L=80,w=5}$	3.58	5.74	7.84	11.92

Moreover, the probability that the degree of i is equal to $d \geq 1$ is $e^{-c}\frac{c^{d-1}}{(d-1)!}$. Hence, we can write,

$$x_{t+1} = \sum_{d=1}^{Q-1} e^{-c}\frac{c^{d-1}}{(d-1)!} + \sum_{d=Q}^{\infty} e^{-c}\frac{c^{d-1}}{(d-1)!}\sum_{j=0}^{Q-2}\binom{d-1}{j}(1-x_t)^j x_t^{d-1-j}. \tag{106}$$

One can simplify this equation. Indeed,

$$\begin{aligned}
1 - x_{t+1} &= \sum_{d=Q}^{\infty} e^{-c}\frac{c^{d-1}}{(d-1)!}\left\{1 - \sum_{j=0}^{Q-2}\binom{d-1}{j}(1-x_t)^j x_t^{d-1-j}\right\} \\
&= \sum_{d=Q}^{\infty} e^{-c}\frac{c^{d-1}}{(d-1)!}\sum_{j=Q-1}^{d-1}\binom{d-1}{j}(1-x_t)^j x_t^{d-1-j} \\
&= e^{-c}\sum_{j=Q-1}^{\infty}\sum_{d=j+1}^{+\infty}\frac{(c(1-x_t))^j}{j!}\frac{(cx_t)^{d-1-j}}{(d-1-j)!} \\
&= e^{-c(1-x_t)}\sum_{j=Q-1}^{\infty}\frac{(c(1-x_t))^j}{j!} \\
&= 1 - e^{-c(1-x_t)}\sum_{j=0}^{Q-2}\frac{c^j}{j!}(1-x_t)^j.
\end{aligned} \tag{107}$$

Defining $y \equiv c(1-x)$ and the function

$$G(y) = 1 - e^{-y}\sum_{j=0}^{Q-2}\frac{y^j}{j!}, \tag{108}$$

we see that we have to study the solutions of the fixed point equation

$$y = c\,G(y). \tag{109}$$

For $c < c_p$ there is a unique trivial fixed point $y = 0$ (i.e., $x = 1$) and the algorithm succeeds. Non-trivial fixed points appear for $c > c_p$ which is the threshold for the emergence of a Q-core. Table 7 contains the numerical values of c_p for several values of Q.

We now take coupled instances from the ensemble defined in Sect. 2. We can write down the density evolution equations and the corresponding one-dimensional fixed point equations. Not surprisingly, similar calculations show that the message passing algorithm is controlled by the one-dimensional fixed point equation,

$$y_z = cG\left(\frac{1}{2w-1}\sum_{k=-w+1}^{w-1} y_{z+k}\right) \tag{110}$$

where $y_z = c(1 - x_z)$ and x_z is the fraction of peeled nodes at position z. Table 7 contains the numerical values of $c_{p,L=80,w=5}$ for several values of Q, and shows the threshold improvement. It can be checked that $c_p \doteq Q$ and $c_{p,L,w} \doteq 2Q$ for $1 \ll w \ll L$. This has to be compared with $c_s \doteq 2Q \ln Q$.

Remark Note that Eqs. (104) and (110) belong to a class of one-dimensional recursions that have recently been analyzed rigorously in [46].

8 Conclusion

In this work we have developed in detail the SP formalism for coupled CSP. We find that the SP thresholds of spatially coupled random K-satisfiability and Q-coloring ensembles nicely saturate towards the SAT-UNSAT phase transition threshold of the individual ensemble. Moreover the SAT-UNSAT phase transition threshold of the coupled and individual ensembles are identical as required by Theorems 1 and 2. The saturation of the SP threshold is remarkably similar to the one of the Belief Propagation algorithmic threshold (towards the optimal one associated to the Maximum a Posteriori decoder) observed in coding theory. We believe that given the set of cavity fixed point equations, it should be possible to prove the observed saturation phenomena by generalizing recent methods developed in the coding context for general channels [3, 4].

Let us point out a few issues that would deserve more investigations, and to which we hope to come back in the future.

The large K and Q analysis has shown that when α is in a small interval where the zero-energy complexity is strictly positive, the warning and complexity densities form kink-like profiles. These are very similar to the kink-like magnetization and free energy densities found in the CW chain. A possible interpretation of the complexity density profiles is that the clusters do not only have a "size" given by their internal entropy but also have a "shape" that could be taken into account by an extension of the entropic cavity method. The simplest system where this issue could be elucidated is the XOR-SAT system for which the clusters can be precisely defined [34]. We hope to come back to this question in the near future.

As briefly discussed in the introduction, the entropic cavity method predicts the existence of other thresholds, namely the dynamical and condensation thresholds. We have checked that the condensation one is the same for a coupled and individual ensemble (for $L \to +\infty$). This observation is consistent with the theorems of Appendix A. We also observe that the dynamical threshold of the coupled ensemble saturates towards the condensation one, for K and $Q \geq 4$. For $K = 3$ the dynamical and condensation thresholds coincide already for the individual ensemble. We consistently observe that they remain unchanged by coupling. These observations deserve more investigations, in particular the nature of the condensed phase, the freezing of variables, the behavior of correlation functions and the possible relevance of the shape of clusters.

The present work could find applications in a new method for proving lower bounds on α_s (and possibly α_c). We hope that by choosing the right analyzable algorithms one may reach significant improvements of the best existing lower bounds. One requirement on the algorithms is that they should be able to propagate in the bulk the "seed" given by the reduced hardness of the coupled instances at their boundaries. We have seen that this is the case for simple peeling-type algorithms which are purely deterministic. Together with D. Achlioptas, we have observed that this is also the case for classic stochastic algorithms if they are augmented by a suitable scheduling [44]. Related ideas have been used recently

within the context of a coupled CSP scheme for source coding [45]. A coupled low-density generator-matrix code is considered, and it is shown (numerically) that applying belief-propagation-guided-decimation with suitable scheduling, allows to approach the optimal rate-distortion curve of the individual code ensemble.

Acknowledgements The work of Hamed Hassani has been supported by Swiss National Science Foundation Grant no 200021-121903. N.M. thanks Marc Mézard and Toshiyuki Tanaka for instructive discussions on coupling for the SK model. We thank Dimitri Achlioptas for interesting discussions on algorithmic aspects.

Appendix A: Free Energy

We sketch the proof of the finite temperature analogs of Theorems 1 and 2. An important consequence is that the free energies of the coupled and individual ensembles have the same singularities in the (α, β) plane (see (118)). This is consistent with the fact that the average ground state energies, and consequently the SAT-UNSAT thresholds, are the same.

The Gibbs distribution (at "inverse temperature" β) associated to the coupled CSP Hamiltonian (3) is

$$\mu_\beta(\underline{x}) = \frac{1}{Z_{\text{cou}}} e^{-\beta \mathcal{H}_{\text{cou}}(\underline{x})}, \quad Z_{\text{cou}} = \sum_{\underline{x}} e^{-\beta \mathcal{H}_{\text{cou}}(\underline{x})}, \tag{111}$$

and the average free energy per node is

$$f_{N,L,w}(\alpha, \beta) = -\frac{1}{\beta L N} \mathbb{E}[\ln Z_{\text{cou}}]. \tag{112}$$

The corresponding quantities $\mathcal{H}^{\text{per}}_{\text{cou}}(\underline{x})$ are associated a chain to with periodic boundary conditions (see Sect. 2); these will be denoted by a superscript "per". Note that to get these quantities for the underlying system, one sets $L = w = 1$ in these definitions; the average free energy per node will be denoted by $f_N(\alpha, \beta)$.

Remark about the entropy The average entropy is defined as

$$s_{N,L,w}(\alpha, \beta) = \frac{\partial}{\partial \beta^{-1}} f_{N,L,w}(\alpha, \beta) = \beta\big(\mathbb{E}\big[\langle \mathcal{H}_{\text{cou}} \rangle\big] - f_{N,L,w}(\alpha, \beta)\big) \tag{113}$$

where $\langle - \rangle$ is the average with respect to (111). Theorems 3 and 4 for the free energy have analogs for the average internal energy, and as a consequence also for the average entropy. Thus the entropy of coupled and individual ensembles have the same singularities in the (α, β) plane. This is consistent with the observation that the condensation threshold at zero temperature is the same for both ensembles.

Theorem 3 (Comparison of open and periodic chains) *For general coupled CSP* $[N, K, \alpha, w, L]$ *ensembles we have*

$$\big| f_{N,L,w}(\alpha, \beta) - f^{\text{per}}_{N,L,w}(\alpha, \beta) \big| \leq \frac{\alpha w}{L}. \tag{114}$$

Proof We write (with the same notations than in the proof of Theorem 1)

$$Z_{\text{cou}} = \sum_{\underline{x}} e^{-\beta \mathcal{H}_{\text{cou}}(\underline{x})} = \sum_{\underline{x}', \underline{x}''} e^{-\beta \mathcal{H}^{\text{per}}_{\text{cou}}(\underline{x}'')} e^{-\beta(\mathcal{H}_{\text{cou}}(\underline{x}', \underline{x}'') - \mathcal{H}^{\text{per}}_{\text{cou}}(\underline{x}''))} \tag{115}$$

and from (77) we deduce

$$e^{-\beta M w} Z_{\text{cou}}^{\text{per}} \le Z_{\text{cou}} \le e^{\beta M w} Z_{\text{cou}}^{\text{per}}. \tag{116}$$

Applying $-\frac{1}{\beta NL}\log$ on each side of this inequality, we obtain the desired estimate. □

Theorem 4 (Comparison of individual and periodic ensembles) *For K-SAT and Q-coloring the limits* $\lim_{N\to+\infty} f_{N,L,w}^{\text{per}}(\alpha,\beta)$ *and* $\lim_{N\to+\infty} f_N(\alpha,\beta)$ *exist, and are continuous in* (α,β), *for all* L. *Moreover,*

$$\lim_{N\to+\infty} f_{N,L,w}^{\text{per}}(\alpha,\beta) = \lim_{N\to+\infty} f_N(\alpha,\beta). \tag{117}$$

Theorems 3 and 4 yield (recall $\lim_{\text{therm}} = \lim_{L\to+\infty}\lim_{N\to+\infty}$)

$$\lim_{\text{therm}} f_{N,L,w}(\alpha,\beta) = \lim_{\text{therm}} f_{N,L,w}^{\text{per}}(\alpha,\beta) = \lim_{N\to+\infty} f_N(\alpha,\beta). \tag{118}$$

Proof The proof of existence and continuity of limits for $N\to+\infty$ (L fixed) is identical to [19], so we do not repeat it here. The proof of the equality uses the same interpolating r-ensembles between the connected, ring and disconnected ensembles defined in Sect. 5.2. The associated Gibbs measures, free energies and expectations will be denoted by scripts r, conn, ring and disc.

By an argument similar to that of Theorem 3 we have the analogs of (83), (84), (85),

$$\begin{cases} -\lim_{N\to+\infty}\frac{1}{\beta LN}\mathbb{E}_{\text{conn}}[\log Z_{\text{conn}}] = \lim_{N\to+\infty} f_N(\alpha,\beta), & \text{for } L \text{ fixed},\\ -\frac{1}{\beta LN}\mathbb{E}_{\text{disc}}[\log Z_{\text{disc}}] = f_N(\alpha,\beta) + O(N^{-1/2}), & \text{uniformly in } L,\\ -\frac{1}{\beta LN}\mathbb{E}_{\text{ring}}[\log Z_{\text{ring}}] = f_{N,L,w}^{\text{per}}(\alpha,\beta) + O(N^{-1/2}), & \text{uniformly in } L. \end{cases}$$

Thus, it is sufficient to show that

$$-\frac{1}{LN}\mathbb{E}_{\text{conn}}[\log Z_{\text{conn}}] \le -\frac{1}{LN}\mathbb{E}_{\text{ring}}[\log Z_{\text{ring}}] \le -\frac{1}{LN}\mathbb{E}_{\text{disc}}[\log Z_{\text{disc}}]. \tag{119}$$

To prove these inequalities we will use the r-ensembles. It suffices to check the analogs of (88) and (96), namely for an intermediate graph $\tilde{G}$,

$$-\big(\mathbb{E}_r[\log Z_{G_r} \mid \tilde{G}] - \log Z_{\tilde{G}}\big) \le -\big(\mathbb{E}_{r-1}[\log Z_{G_{r-1}} \mid \tilde{G}] - \log Z_{\tilde{G}}\big), \tag{120}$$

and then average over $\tilde{G}$.

Consider the graph $\tilde{G}$ and add a new constraint node n to it. The precise way in which n is connected to the variable nodes is deferred to a later stage of the argument. We have

$$\frac{Z_{\tilde{G}\cup n}}{Z_{\tilde{G}}} = e^{-\beta} \sum_{\underline{x}:\, n \text{ is UNSAT}} \mu_{\beta,\tilde{G}}(\underline{x}) + \sum_{\underline{x}:\, n \text{ is SAT}} \mu_{\beta,\tilde{G}}(\underline{x}). \tag{121}$$

This is equivalent to

$$\frac{Z_{\tilde{G}\cup n}}{Z_{\tilde{G}}} = 1 - \big(1-e^{-\beta}\big) \sum_{\underline{x}:\, n \text{ is UNSAT}} \mu_{\beta,\tilde{G}}(\underline{x}). \tag{122}$$

Taking the log and expectation over n for a given $\tilde{G}$, we obtain

$$-\mathbb{E}\left[\log\frac{Z_{\tilde{G}\cup n}}{Z_{\tilde{G}}}\,\middle|\,\tilde{G}\right] = -\mathbb{E}\left[\log\left\{1-\big(1-e^{-\beta}\big)\sum_{\underline{x}:\, n \text{ is UNSAT}}\mu_{\beta,\tilde{G}}(\underline{x})\right\}\,\middle|\,\tilde{G}\right]. \tag{123}$$

Note that the left hand side is identical to that of (120). To compute the expectation we expand $-\log(1-x) = \sum_{l\geq 1} \frac{x^l}{l}$,

$$-\mathbb{E}\Big[\log \frac{Z_{\tilde{G}\cup n}}{Z_{\tilde{G}}} \;\Big|\; \tilde{G}\Big] = \sum_{l\geq 1} \frac{(1-e^{-\beta})^l}{l} \times \mathbb{E}\Big[\sum_{\underline{x}^{(1)},\dots,\underline{x}^{(l)}:\, n \text{ is UNSAT}} \mu_{\beta,\tilde{G}}\big(\underline{x}^{(1)}\big)\dots\mu_{\beta,\tilde{G}}\big(\underline{x}^{(l)}\big)\} \;\Big|\; \tilde{G}\Big]. \quad (124)$$

The sum over "real replicas" $\underline{x}^{(1)},\dots,x^{(l)}$ is over assignments such that n is UNSAT for all l of them, so the expectation in (124) equals

$$\frac{1}{Z_{\tilde{G}}^l} \sum_{\underline{x}^{(1)},\dots,\underline{x}^{(l)}} e^{-\beta\sum_{\rho=1}^{l}\mathcal{H}_{\tilde{G}}(\underline{x}^{(\rho)})}\mathbb{E}\big[\mathbb{1}\{n \text{ UNSAT on all } \underline{x}^{(\rho)}, h=1,\dots,l\} \;\big|\; \tilde{G}\big]. \quad (125)$$

Up to this stage the arguments are completely general: they apply both to coloring and satisfiability. We specialize the rest of the proof to K-SAT and leave coloring as an exercise.

We first derive (120) for the r-ensemble that interpolates between the *connected and ring* ensembles. This then implies the left inequality in (119). Given $\tilde{G}$ and given a term $\underline{x}^{(1)},\dots,x^{(l)}$ in (125), let $\mathcal{F}$ be the set of variable nodes with frozen bits, i.e. those variable nodes such that the bit takes the same value in all assignments $\underline{x}^{(1)}$ through $\underline{x}^{(l)}$. Below we will also need the sets $\mathcal{F}_z = \mathcal{F}\cap V_z$. When n is connected u.a.r. to the LN variable nodes we go from $\tilde{G}$ to a G_r graph and

$$\mathbb{E}_r\big[\mathbb{1}\{n \text{ UNSAT on all } \underline{x}^{(\rho)}, h=1,\dots,l\} \;\big|\; \tilde{G}\big] = \frac{1}{2^K}\left(\frac{|\mathcal{F}|}{LN}\right)^K. \quad (126)$$

On other hand when n is first affected u.a.r. to a position z and then connected u.a.r. to the wN variables in $\bigcup_{k=0}^{w-1} V_{z+k \bmod L}$, we go from $\tilde{G}$ to a G_{r-1} graph and

$$\mathbb{E}_{r-1}\big[\mathbb{1}\{n \text{ UNSAT on all } \underline{x}^{(\rho)}, h=1,\dots,l\} \;\big|\; \tilde{G}\big] = \frac{1}{L}\sum_{z=-\frac{L}{2}+1}^{\frac{L}{2}} \frac{1}{2^K}\left(\frac{1}{wN}\sum_{k=0}^{w-1}|\mathcal{F}_{z+k \bmod L}|\right)^K. \quad (127)$$

By convexity, the quantity in (126) is smaller than the one in (127). Using this fact together with (123), (124), (125), we obtain the final inequality (120). This implies the left inequality in (119).

The derivation of (120) for the r-ensemble that interpolates between the *ring and disconnected* ensembles is similar. When n is first affected u.a.r. to a position z, and then connected u.a.r. to N variable nodes in the set V_z we go from $\tilde{G}$ to a G_{r-1} graph. Thus,

$$\mathbb{E}_{r-1}\big[\mathbb{1}\{n \text{ UNSAT on all } \underline{x}^{(\rho)}, h=1,\dots,l\} \;\big|\; \tilde{G}\big] = \frac{1}{L}\sum_{z=-\frac{L}{2}+1}^{\frac{L}{2}} \frac{1}{2^K}\left(\frac{|\mathcal{F}_z|}{N}\right)^K. \quad (128)$$

Finally we notice that by convexity, (127) is smaller than (128), so that using again (123), (124) and (125) we obtain the final inequality (120). This now implies the right inequality in (119). □

We now turn to the case of XORSAT which has to be treated somewhat differently. All definitions of average ground state energies and free energies are the same as usual.

Theorem 5 (Energy comparisons for XORSAT) *For K-XORSAT with even K the limits $\lim_{N\to+\infty} f^{\text{per}}_{N,L,w}(\alpha,\beta)$ and $\lim_{N\to+\infty} f_N(\alpha,\beta)$ exist, are continuous in (α,β), and are equal. The same holds for the zero temperature quantities, i.e. for $\lim_{N\to+\infty} e^{\text{per}}_{N,L,w}(\alpha)$ and $\lim_{N\to+\infty} e_N(\alpha)$.*

Proof Existence and continuity of the limits for K-XORSAT follows from sub-additivity which was already proven in [18] for K even.[9] Here we concentrate on the equality of limits. The proof uses exactly the same interpolations as in the proof of Theorem 4.

First we prove the same relation as in (119) for the case of XORSAT. For this we proceed exactly as in Eqs. (120)–(125) and reduce the problem to estimating the expectation

$$\mathbb{E}\big[\mathbb{1}\big\{n \text{ UNSAT on all } \underline{x}^{(\rho)}, \rho = 1,\dots,l\big\} \,\big|\, \tilde{G}\big], \tag{129}$$

according to the various ways of connecting the new constraint node n. It will be useful to represent the indicator function in an algebraic way.[10] Suppose that n connects to variable nodes $n_1,\dots,n_K$, then

$$\mathbb{1}\big\{n \text{ UNSAT on all } \underline{x}^{(\rho)}, \rho = 1,\dots,l\big\} = \prod_{\rho=1}^{l} \frac{1}{2}\left(1 - b_n \prod_{v=1}^{K} (-1)^{x_{n_v}^{(\rho)}}\right)$$

$$= \frac{1}{2^l} \sum_{0\le r\le l} (-1)^r b_n^r \sum_{\{\rho_1,\dots,\rho_r\}\subset\{1,\dots,l\}} \prod_{v=1}^{K} \big\{(-1)^{x_{n_v}^{(\rho_1)}} \dots (-1)^{x_{n_v}^{(\rho_r)}}\big\}. \tag{130}$$

When we take the expectation over $b_n \sim \text{Bernoulli}(1/2)$ only the terms with r even remain,

$$\frac{1}{2^l} \sum_{0\le r\le l}^{r\,\text{even}} \sum_{\{\rho_1,\dots,\rho_r\}\subset\{1,\dots,l\}} \prod_{v=1}^{K} \big\{(-1)^{x_{n_v}^{(\rho_1)}} \dots (-1)^{x_{n_v}^{(\rho_r)}}\big\}. \tag{131}$$

Now, it remains to compute the rest of the expectation on possible ways of connecting n. We define "local overlap parameters"

$$Q_z^{(\rho_1,\dots,\rho_l)} = \frac{1}{N} \sum_{i=1}^{N} (-1)^{x_{iz}^{(\rho_1)}} \dots (-1)^{x_{iz}^{(\rho_r)}}. \tag{132}$$

Let us first consider the interpolation between the *ring and fully connected* ensembles. To go from $\tilde{G}$ to G_r we connect n u.a.r. among all LN variable nodes $v = (i,z)$. Thus (129) becomes

$$\frac{1}{2^l} \sum_{0\le r\le l}^{r\,\text{even}} \sum_{\{\rho_1,\dots,\rho_r\}\subset\{1,\dots,l\}} \left\{\frac{1}{L} \sum_{z=-\frac{L}{2}+1}^{\frac{L}{2}} Q_z^{(\rho_1,\dots,\rho_l)}\right\}^K. \tag{133}$$

[9] The argument in [18] covers also K-SAT for even K, but a small modification of it extends the proof to odd K; however for XORSAT with odd K it not clear how to extend the proof. Strangely enough, another case were such arguments break down is that of pure ferromagnetic diluted interactions.

[10] The method used here can be used also for satisfiability and coloring and although it is somewhat longer, it may be useful when it is not obvious how to define "frozen variables".

On the other hand to go from $\tilde{G}$ to G_{r-1}, we first affect n to a position z u.a.r. and connect its K edges to variable nodes $v = (i, z + k)$ with $k \in \{0, \dots w - 1\}$ u.a.r.. This time (129) becomes

$$\frac{1}{2^l} \sum_{0 \le r \le l}^{r \text{ even}} \sum_{\{\rho_1, \dots, \rho_r\} \subset \{1, \dots, l\}} \frac{1}{L} \sum_{z=-\frac{L}{2}+1}^{\frac{L}{2}} \left\{ \frac{1}{w} \sum_{k=0}^{w-1} Q_{z+k \bmod L}^{(\rho_1, \dots, \rho_l)} \right\}^K . \tag{134}$$

Convexity of the function x^K for even K implies that (133) $\le$ (134), which then implies the left inequality in (119). Unfortunately at this point the argument breaks down for odd K because we do not control the sign of the overlap parameters.

Consider now the interpolation between the *ring and disconnected* ensembles. When the extra node is first affected to z u.a.r. and its K edges connected u.a.r. to the N variable nodes at the same position, we obtain for (129)

$$\frac{1}{2^l} \sum_{0 \le r \le l}^{r \text{ even}} \sum_{\{\rho_1, \dots, \rho_r\} \subset \{1, \dots, l\}} \frac{1}{L} \sum_{z=-\frac{L}{2}+1}^{\frac{L}{2}} \left\{ Q_z^{(\rho_1, \dots, \rho_l)} \right\}^K . \tag{135}$$

Again convexity of x^K for K even implies that (134) $\le$ (135), which then implies the right inequality in (119).

We have proven (119) for any finite β, and since L and N are finite, there is no difficulty in taking the $\beta \to +\infty$ limit. This yields the zero temperature version of this inequality, namely (86) applied to XORSAT.

Finally with the help of (86) and (119) we conclude (proceeding as in the previous proofs) that the average ground state and free energies of the individual and periodic ensemble are equal in the limit $N \to +\infty$, with L and w fixed. □

Appendix B: Review of the Cavity Method and Survey Propagation Equations

The main assumptions of the cavity method draw on the concept of pure (or extremal or ergodic) state. While this concept can be given a rigorous meaning for "simple" models [30, 31], it still forms a heuristic framework in the context of disordered spin systems. We refer the interested reader to [12, 36–39] for more information and various approaches.

Infinite volume Gibbs measures form a convex set whose extremal points play a special role and are called *pure states*. A crucial property of a pure state is that the correlations decay (usually exponentially fast) with the graph distance. This is not true for non-trivial convex superpositions of pure states. For "simple" Ising-type models the number of pure states is "small" and they are related by a broken symmetry. Disordered spin systems can have an exponential (in system size) number of pure states and the broken symmetry, if only there exist one, is hard to identify.[11] The growth rate of the number of pure states, is called the complexity. This is a notion analogous to the Boltzmann entropy, but at the level of pure states, instead of microscopic configurations, for which one develops a new "level" of statistical mechanics.

We assume that this picture can be taken over to CSP and even coupled-CSP. Let p index the set of pure states (we called them pure Bethe states in Sect. 2). The special feature about systems on random graphs is that they are locally tree-like with high probability. Thus, since

[11] Within the replica formalism it is a formal symmetry between "a number" of copies of the system.

for each pure state p the correlations decay sufficiently fast, in order to compute the one-point marginals at a vertex *of the pure state* p one restricts the measure to the local tree around the vertex. The statistical mechanical sums on the tree can be performed recursively so that the one-point marginal at the vertex is computed from a set of "messages" satisfying the so-called sum-product (or Belief Propagation) equations

$$\hat{\nu}^{(p)}_{cz\to iu}(x_{iu}) \cong \sum_{x_{\partial(cz)\setminus iu}} \psi_{cz}(x_{\partial(cz)}) \prod_{jv\in\partial(cz)\setminus iu} \nu^{(p)}_{jv\to cz}(x_{jv}), \tag{136}$$

$$\nu^{(p)}_{iu\to cz}(x_{iu}) \cong \prod_{bv\in\partial(iu)\setminus cz} \hat{\nu}^{(p)}_{bv\to iu}(x_{iu}). \tag{137}$$

In (136), (137) $\cong$ means that the right hand side has to be divided by a normalization factor to get a true marginal on the left. The free energy of the pure state p is given by the Bethe expression,

$$\begin{aligned}\beta F^{(p)} = &\sum_{cz} \ln\Big\{\sum_{x_{\partial(cz)}} \psi_{cz}(x_{\partial(cz)}) \prod_{iu\in\partial(cz)} \nu^{(p)}_{iu\to cz}(x_{iu})\Big\}\\ &+\sum_{iu} \ln\Big\{\sum_{x_{iu}} \prod_{cz\in\partial(iu)} \hat{\nu}^{(p)}_{cz\to iu}(x_{iu})\Big\}\\ &-\sum_{\langle cz,iu\rangle\in E} \ln\Big\{\sum_{x_{iu}} \nu^{(p)}_{iu\to cz}(x_{iu})\hat{\nu}^{(p)}_{cz\to iu}(x_{iu})\Big\}.\end{aligned} \tag{138}$$

To investigate the zero temperature limit $\beta\to+\infty$ we set

$$\nu^{(p)}_{iu\to cz}(x_{iu}) = \frac{e^{-\beta E^{(p)}_{iu\to cz}(x_{iu})}}{\sum_{x_{iu}\in\mathcal{X}} e^{-\beta E^{(p)}_{iu\to cz}(x_{iu})}}, \qquad \hat{\nu}^{(p)}_{cz\to iu}(x_{iu}) = \frac{e^{-\beta \hat{E}^{(p)}_{cz\to iu}(x_{iu})}}{\sum_{x_{iu}\in\mathcal{X}} e^{-\beta \hat{E}^{(p)}_{cz\to iu}(x_{iu})}}. \tag{139}$$

When $\beta\to\infty$, the sum-product equations (136) and (137) reduce to the min-sum equations

$$\begin{aligned}E_{iu\to cz}(x_{iu}) &= \min\Big\{1, \sum_{bv\in\partial(iu)\setminus cz} \hat{E}_{bv\to iu}(x_{iu}) - C_{iu\to cz}\Big\}\\ &\equiv \mathcal{G}_{iu\to cz}\big[\{\hat{E}_{bv\to iu}\}_{bv\in\partial(iu)\setminus cz}\big],\end{aligned} \tag{140}$$

$$\begin{aligned}\hat{E}_{cz\to iu}(x_{iu}) &= \min_{x_{\partial cz\setminus iu}}\Big\{\big(1-\psi_{cz}(x_{\partial(cz)})\big) + \sum_{jv\in\partial(cz)\setminus iu} E_{jv\to cz}(x_j)\Big\} - \hat{C}_{cz\to iu}\\ &\equiv \hat{\mathcal{G}}_{cz\to iu}\big[\{E_{jv\to cz}\}_{jv\in\partial(cz)\setminus iu}\big].\end{aligned} \tag{141}$$

Here, $C_{iu\to cz}$ and $\hat{C}_{cz\to iu}$ are normalization constants fixed so that $\min_{x_{iu}} E_{iu\to cz}(x_{iu}) = \min_{x_{iu}} E_{cz\to iu}(x_{iu}) = 0$. The Bethe formula for the free energy of a pure state reduces to an expression for its ground-state energy

$$\lim_{\beta\to+\infty} \beta F^{(p)} = \mathcal{E}\big[\big\{E^{(p)}_{iu\to cz}(.), E^{(p)}_{cz\to iu}(.)\big\}\big], \tag{142}$$

where the functional $\mathcal{E}$ is given by

$$\begin{aligned}\mathcal{E}\big[\{E_{iu\to cz}, E_{cz\to iu}\}\big] &= \sum_{cz}\min_{x_{\partial(cz)}}\Big\{\big(1-\psi_{cz}(x_{\partial(cz)})\big)+\sum_{iu\in\partial(cz)}E_{iu\to cz}(x_{iu})\Big\}\\ &\quad+\sum_{iu}\min_{x_{iu}}\Big\{\sum_{cz\in\partial iu}\hat{E}_{cz\to iu}(x_{iu})\Big\}\\ &\quad-\sum_{\langle cz,iu\rangle}\min_{x_{iu}}\big\{E_{iu\to cz}(x_{iu})+\hat{E}_{cz\to iu}(x_{iu})\big\}\\ &\equiv\sum_{cz}\mathcal{E}_{cz}\big[\{E_{iu\to cz}\}_{iu\in\partial cz}\big]+\sum_{iu}\mathcal{E}_{iu}\big[\{\hat{E}_{cz\to iu}\}_{cz\in\partial iu}\big]\\ &\quad-\sum_{\langle cz,iu\rangle}\mathcal{E}_{cz,iu}\big[\{E_{iu\to cz},\hat{E}_{cz\to iu}\}\big].\end{aligned}\tag{143}$$

We assume that the heuristic low temperature picture carries over to the zero temperature case. In this context pure states become clusters (in Hamming space) of minimizers of the Hamiltonian. Each cluster is characterized by a set of messages $\{E^{(p)}_{iu\to cz}(.), E^{(p)}_{cz\to iu}(.)\}$. At zero temperature, two minimizers belonging to the same cluster can be connected by successive flips with infinitesimal energy cost, while for two minimizers belonging to different clusters this is not possible.

Now we wish to compute the complexity (15) which counts the number of clusters. For this we introduce a generating function

$$\Xi(y)=\sum_{p}e^{-y\mathcal{E}[\{E^{(p)}_{iu\to cz}(.),E^{(p)}_{cz\to iu}(.)\}]}.\tag{144}$$

When $y\to+\infty$ the sum is dominated by solutions of the min-sum equations with minimal Bethe energy. This object can be viewed as a partition function for the effective Hamiltonian (143) at inverse "temperature" y (the so-called Parisi parameter). Now, if we take α in the SAT phase the minimum Bethe energy vanishes and the complexity (15) is given by

$$\Sigma_{L,w}(\alpha)=\lim_{y\to+\infty}\lim_{N\to+\infty}\frac{1}{NL}\ln\Xi(y).\tag{145}$$

A negative complexity signals that there are no zero energy states and that the system is in an UNSAT phase. When this happens one has to generalize these formulas to allow for an energy dependent complexity (obtained by the Legendre transform of $\ln\Xi(y)$) but this aspect will not concern us here. For CSP's it can be shown that the min-sum messages take discrete values in a finite alphabet. Therefore we have

$$\begin{aligned}\Xi(y)=&\sum_{\{E_{iu\to cz},\hat{E}_{cz\to iu}\}}\Big\{\prod_{\langle iu,cz\rangle}e^{+y\mathcal{E}_{cz,iu}}\Big\}\prod_{iu}\Big\{e^{-y\mathcal{E}_{iu}}\prod_{cz\in\partial(iu)}\mathbb{1}(E_{iu\to cz}=\mathcal{G}_{iu\to cz})\Big\}\\ &\times\prod_{cz}\Big\{e^{-y\mathcal{E}_{cz}}\prod_{iu\in\partial(cz)}\mathbb{1}(\hat{E}_{cz\to iu}=\hat{\mathcal{G}}_{cz\to iu})\Big\}.\end{aligned}\tag{146}$$

The arguments of the functionals $\mathcal{E}_{iu}[-]$, $\mathcal{E}_{cz}[-]$, $\mathcal{E}_{iu,cz}[-]$ and $\mathcal{G}_{iu\to cz}[-]$, $\hat{\mathcal{G}}_{cz\to iu}[-]$ are the messages $\{E_{iu\to cz}(.),\hat{E}_{cz\to iu}(.)\}$; they are not explicitly written to ease the notation. It can easily be seen that this is the partition function of a new graphical model which is still sparse. Edges $\langle(c,z),(i,u)\rangle$ now correspond to degree two "constraint" nodes, and nodes (c,z) and (i,u) now correspond to "variable" nodes. Therefore (145) can be computed from the Bethe approximation for this new model. The underlying assumption here is

that the new effective model has a unique "pure state" with fast decaying correlations. This is called the level-1 cavity method. If this assumption breaks down, one should repeat the whole scheme, obtaining a level-2 cavity method (and so on). At level-1, the Bethe approximation can be expressed in terms of new beliefs—called *surveys*—$Q_{iu\to cz}(E_{iu\to cz}(.))$ and $\hat{Q}_{cz\to iu}(\hat{E}_{cz\to iu}(.))$ that count the *fraction of clusters* p for which $E^{(p)}_{iu\to cz}(.) = E_{iu\to cz}(.)$ and $E^{(p)}_{cz\to iu}(.) = E_{cz\to iu}(.)$. Note that these are the messages on the induced graph obtained by eliminating the degree two constraint nodes of the new model. We have

$$\begin{aligned}\ln \Xi(y) = &\sum_{cz} \ln\Bigg\{ \sum_{\{E_{iu\to cz}\}_{iu\in\partial(cz)}} e^{-y\mathcal{E}_{cz}} \prod_{iu\in\partial cz} Q_{iu\to cz} \Bigg\} \\ &+ \sum_{iu} \ln\Bigg\{ \sum_{\{\hat{E}_{cz\to iu}\}_{cz\in\partial(iu)}} e^{-y\mathcal{E}_{iu}} \prod_{cz\in\partial iu} Q_{cz\to iu} \Bigg\} \\ &- \sum_{cz,iu} \ln\Bigg\{ \sum_{E_{iu\to cz},\hat{E}_{cz\to iu}} e^{-y\mathcal{E}_{iu,cz}} Q_{iu\to cz}\hat{Q}_{cz\to iu} \Bigg\}. \end{aligned} \tag{147}$$

The messages satisfy the *survey propagation equations*

$$\begin{aligned} Q_{iu\to cz}(E_{iu\to cz}) \cong &\sum_{\{\hat{E}_{bv\to iu}\}_{cz\in\partial(iu)}} \mathbb{1}(E_{iu\to cz} = \mathcal{G}_{iu\to cz}) e^{-yC_{iu\to cz}} \\ &\times \prod_{bv\in\partial(iu)\setminus cz} Q_{bv\to iu}(\hat{E}_{bv\to iu}), \end{aligned} \tag{148}$$

$$\begin{aligned} \hat{Q}_{cz\to iu}(\hat{E}_{cz\to iu}) \cong &\sum_{\{\hat{E}_{jv\to cz}\}_{jv\in\partial(cz)}} \mathbb{1}(\hat{E}_{cz\to iu} = \hat{\mathcal{G}}_{cz\to iu}) e^{-y\hat{C}_{cz\to iu}} \\ &\times \prod_{jv\in\partial(cz)\setminus iu} Q_{jv\to cz}(E_{jv\to cz}), \end{aligned} \tag{149}$$

where again $\cong$ means that the right hand side has to be normalized.

In the SAT phase one takes $y \to +\infty$ in order to compute the complexity. This has the effect of reducing the sums in (148), (149) and (147), to surveys such that $C_{iu\to cz} = \hat{C}_{cz\to iu} = 0$ and $\mathcal{E}_{cz} = \mathcal{E}_{iu} = \mathcal{E}_{iu,cz} = 0$.

References

1. Felstrom, A., Zigangirov, K.S.: Time-varying periodic convolutional codes with low density parity check matrix. IEEE Trans. Inf. Theory **45**(5), 2181–2190 (1999)
2. Kudekar, S., Richardson, T., Urbanke, R.: Threshold saturation via spatial coupling: why convolutional LDPC ensembles perform so well over the BEC. IEEE Trans. Inf. Theory **57**, 803–834 (2011)
3. Kudekar, S., Richardson, T., Urbanke, R.: Spatially coupled ensembles universally achieve capacity under belief propagation. In: International Symposium on Information Theory Proceedings, pp. 453–457 (2012). See also arXiv:1201.2999v1 [cs.IT]
4. Kumar, S., Young, A.J., Macris, N., Pfister, H.D.: A proof of threshold saturation for irregular LDPC codes on BMS channels. In: Proc. of 50th Annual Allerton Conference on Communication, Control, and Computing (October 2012)
5. Hassani, S.H., Macris, N., Urbanke, R.: Coupled graphical models and their threshold. In: Proceedings IEEE Information Theory Workshop (ITW), Dublin, pp. 1–5 (2010). arXiv:1105.0785v1 [cs.IT]
6. Hassani, S.H., Macris, N., Urbanke, R.: Chains of mean field models. J. Stat. Mech. **2012**, P02011 (2012)
7. Bak, P.: Commensurate phases, incommensurate phases and the devils staircase. Rep. Prog. Phys. **45**, 587–629 (1982)

8. Krug, J., Lebowitz, J.L., Spohn, H., Zhang, M.Q.: The fast rate limit of driven diffusive systems. J. Stat. Phys. **44**, 535 (1986)
9. Kudekar, S., Pfister, H.D.: The effect of spatial coupling on compressive sensing. In: 48th Annual Allerton Conference, pp. 347–353 (2010)
10. Krzakala, F., Mézard, M., Sausset, F., Sun, Y., Zdeborova, L.: Statistical physics-based reconstruction in compressed sensing. Phys. Rev. X **2**, 021005 (2012)
11. Donoho, D.L., Javanmard, A., Montanari, A.: Information-theoretically optimal compressed sensing via spatial coupling and approximate message passing. arXiv:1112.0708v1 [cs.IT]. See also: IEEE International Symposium on Information Theory Proceedings, pp. 1231–1235 (2012)
12. Mézard, M., Montanari, A.: Information, Computation and Physics. Oxford University Press, London (2010)
13. Mézard, M., Parisi, G.: The cavity method at zero temperature. J. Stat. Phys. **111**(1–2), 1–34 (2003).
14. Mézard, M., Parisi, G., Zecchina, R.: Analytic and algorithmic solution of random satisfiability problems. Science **297**, 812–815 (2002)
15. Mézard, M., Zecchina, R.: Random K-satisfiability problem: from an analytic solution to an efficient algorithm. Phys. Rev. E **66**, 056126 (2002)
16. Guerra, F., Toninelli, F.: The thermodynamic limit in mean field spin glass models. Commun. Math. Phys. **203**, 71–79 (2002)
17. Guerra, F., Toninelli, F.: The high temperature region of the Viana-Bray diluted spin glass model. J. Stat. Phys. **115**, 531–555 (2004)
18. Franz, S., Leone, M.: Replica bounds for optimization problems and diluted spin glass problems. J. Stat. Phys. **111**, 535–564 (2003)
19. Bayati, M., Gamarnik, D., Tetali, P.: Combinatorial approach to the interpolation method and scaling limits in sparse random graphs. In: Proceedings STOC, pp. 105–114 (2010)
20. Mézard, M., Palassini, M., Rivoire, O.: Landscape of solutions in constraint satisfaction problems. Phys. Rev. Lett. **95**, 200202 (2005)
21. Zdeborova, L., Krzakala, F.: Phase transitions in the coloring of random graphs. Phys. Rev. E **76**, 031131 (2007)
22. Montanari, A., Ricci-Tersenghi, F., Semerjian, G.: Clusters of solutions and replica symmetry breaking in random K-satisfiability. J. Stat. Mech. Theory Exp. **2008**, P04004 (2008)
23. Krzakala, F., Montanari, A., Ricci-Tersenghi, F., Semerjian, G., Zdeborova, L.: Gibbs states and the set of solutions of random constraint satisfaction problems. Proc. Natl. Acad. Sci. **104**, 10318–10323 (2007)
24. Ricci-Tersenghi, F., Sermerjian, G.: On the cavity method for decimated random constraint satisfaction problems and the analysis of belief propagation guided decimation algorithms. J. Stat. Mech. **2009**, P09001 (2009)
25. Coja-Oglhan, A.: On belief propagation guided decimation for random K-SAT. In: Proc. 22nd SODA, pp. 957–966 (2011)
26. Kirkpatrick, T.R., Wolynes, P.G.: Connections between some kinetic and equilibrium theories of the glass transition. Phys. Rev. A **35**, 3072–3080 (1987)
27. Kirkpatrick, T.R., Thirumalai, D.: p-Spin interaction spin glass models: connections with the structural glass problem. Phys. Rev. B **36**, 5388–5397 (1987)
28. Berthier, L., Biroli, G.: Theoretical perspective on the glass transition and amorphous materials. Rev. Mod. Phys. **83**, 587–645 (2011)
29. Abbe, E., Montanari, A.: On the concentration of the number of solutions of random satisfiability formulas. arXiv:1006.3786v1
30. Ruelle, D.: Statistical Mechanics: Rigorous Results. Mathematical Series Monograph Series. Benjamin, Amsterdam (1983)
31. Georgii, H.O.: Gibbs Measures and Phase Transitions. De Gruyter Studies in Mathematics, vol. 9. de Gruyter, Berlin (1988)
32. Franco, J.: Probabilistic analysis of the pure literal heuristic for the satisfiability problem. Ann. Oper. Res. **1**, 273–289 (1984)
33. Broder, A.Z., Frieze, A.M., Upfal, E.: On the satisfiability and maximum satisfiability of random 3-CNF formulas. In: 4th Annual ACM-SIAM Symposium on Discrete Algorithms, Austin, TX, 1993, pp. 322–330. ACM, New York (1993)
34. Mézard, M., Ricci-Tersenghi, F., Zecchina, R.: Two solutions to diluted p-spin models and XORSAT problems. J. Stat. Phys. **111**, 505–533 (2003)
35. Pittel, B., Spencer, J., Wormald, N.: Sudden emergence of a giant k-core in a random graph. J. Comb. Theory Ser. B **67**, 111–151 (1996)
36. Mézard, M., Parisi, G., Virasoro, M.A.: Spin Glass Theory and Beyond. World Scientific, Singapore (1987)
37. Talagrand, M.: Spin Glasses: A Challenge for Mathematicians. Springer, Berlin (2000)

38. Stein, D.L., Newman, C.: Thermodynamic chaos and the structure of short-range spin glasses. In: Bovier, A., Picco, P. (eds.) Mathematics of Spin Glasses and Neural Networks, pp. 243–247. Birkhäuser, Boston (1998)
39. Aizenman, M., Wehr, J.: Rounding effects of quenched randomness on first-order phase transitions. Commun. Math. Phys. **130**, 489–528 (1990)
40. Luby, M., Mitzenmacher, M., Shokrollahi, A.: Analysis of random processes via And-Or trees. In: Proceeding of the Ninth Annual ACM-SIAM Symposium on Discrete Algorithms (1998)
41. Mertens, S., Mézard, M., Zecchina, R.: Threshold values of random K-SAT from the cavity method. Random Struct. Algorithms **28**, 340–373 (2006)
42. Kudekar, S., Richardson, T., Urbanke, R.: Wave-like solutions of general one-dimensional spatially coupled systems. arXiv:1208.5273 [cs.IT]
43. Mulet, R., Pagnani, A., Weigt, M., Zecchina, R.: Coloring random graphs. Phys. Rev. Lett. **89**, 268701 (2002)
44. Achlioptas, D., Hassani, H., Macris, N., Urbanke, R.: Work in progress
45. Aref, V., Macris, N., Urbanke, R., Vuffray, M.: Lossy source coding via spatially coupled LDGM ensembles. In: International Symposium on Information Theory Proceedings, pp. 373–377 (2012). arXiv:1202.4959v1 [cs.IT]
46. Yedla, A., Jian, Y., Nguyen, P.S., Pfister, H.D.: A simple proof of threshold saturation for coupled scalar recursions. In: Proceedings of Int. Symp. on Turbo Codes and Iterative Information Processing. arXiv:1204.5703